Article

Identification of Infiltration Features and Hydraulic Properties of Soils Based on Crop Water Stress Derived from Remotely Sensed Data

Jakub Brom [1,*], **Renata Duffková** [2], **Jan Haberle** [3], **Antonín Zajíček** [2], **Václav Nedbal** [1], **Tereza Bernasová** [1], **Kateřina Křováková** [1]

1   Faculty of Agriculture, University of South Bohemia in České Budějovice, Studentská 1668, 370 05 České Budějovice, Czech Republic; nedbav00@zf.jcu.cz (V.N.); veselt04@zf.jcu.cz (T.B.); krovak00@jcu.cz (K.K.)
2   Research Institute for Soil and Water Conservation, Žabovřeská 250, 156 27 Praha 5-Zbraslav, Czech Republic; duffkova.renata@vumop.cz (R.D.); zajicek.antonin@vumop.cz (A.Z.)
3   Crop Research Institute, Drnovská 507/73, 161 06 Praha 6-Ruzyně, Czech Republic; haberle@vurv.cz
*   Correspondence: jbrom@zf.jcu.cz

Abstract: Knowledge of the spatial variability of soil hydraulic properties is important for many reasons, e.g., for soil erosion protection, or the assessment of surface and subsurface runoff. Nowadays, precision agriculture is gaining importance for which knowledge of soil hydraulic properties is essential, especially when it comes to the optimization of nitrogen fertilization. The present work aimed to exploit the ability of vegetation cover to identify the spatial variability of soil hydraulic properties through the expression of water stress. The assessment of the spatial distribution of saturated soil hydraulic conductivity (K_s) and field water capacity (*FWC*) was based on a combination of ground-based measurements and thermal and hyperspectral airborne imaging data. The crop water stress index (CWSI) was used as an indicator of crop water stress to assess the hydraulic properties of the soil. Supplementary vegetation indices were used. The support vector regression (SVR) method was used to estimate soil hydraulic properties from aerial data. Data analysis showed that the approach estimated K_s with good results ($R^2 = 0.77$) for stands with developed crop water stress. The regression coefficient values for estimation of *FWC* for topsoil (0–0.3 m) ranged from $R^2 = 0.38$ to $R^2 = 0.99$. The differences within the study sites of the *FWC* estimations were higher for the subsoil layer (0.3–0.6 m). R^2 values ranged from 0.12 to 0.99. Several factors affect the quality of the soil hydraulic features estimation, such as crop water stress development, condition of the crops, period and time of imaging, etc. The above approach is useful for practical applications for its relative simplicity, especially in precision agriculture.

Keywords: soil infiltration; field water capacity; crop water stress; machine learning; aerial remote sensing; precision agriculture

1. Introduction

The soil hydraulic properties (hydraulic conductivity and water retention characteristics) play a key role in many agro-environmental processes (e.g., nutrient leaching or soil erosion) and soil management practices [1]. They affect the rate of water infiltration into the soil and partitioning precipitation into surface and subsurface runoff, groundwater recharge, evapotranspiration and soil moisture content [2]. When the rainfall intensity exceeds the soil saturation capacity, a surface runoff mechanism and soil erosion process are initiated [3].

Soil saturated hydraulic conductivity (K_s) describes the process of water movement in the soil profile. It is affected by rainfall intensity, the share and continuity of macropores and particle size distribution (the proportion of sand, silt and clay); therefore K_s tends to be spatially and temporally variable [4,5]. More drained sandy soils have relatively high

K_s compared to clayey soils because most pores drain shortly after rainfall or irrigation, indicating low soil retention capacity, also known as field water capacity (*FWC*) [6].

The spatial heterogeneity of soil hydraulic properties directly affects crop yields via air-filled porosity, plant available water and penetration of plant roots [7]. Implementing soil heterogeneity into site-specific farming practices, increasing the efficiency of agricultural inputs, is a prerequisite for the use of precision agriculture methods [8,9]. The manifestation of soil heterogeneity is enhanced by plant water stress. It should be incorporated into the functional characteristics that determine an efficient management strategy for precision agriculture [8]. Variable-rate fertilization as one of the precision agriculture techniques is based on the delineation of 'management zones' that express sub-areas with homogeneous yield potential [10,11]. This strategy is mainly applied to introduce more efficient management of nitrogen fertilizers via reducing their over-consumption, while maintaining crop yield [12,13]. In addition, the application of locally adapted nitrogen fertilizer rates has excellent potential to reduce nitrate leaching to ground and surface water in areas with a high K_s and low *FWC*. This is highly desirable because arable land contributes significantly to nitrate pollution in the catchment [14]. From a hydrogeological point of view, nitrogen leaching in a basin is controlled by the functions of the so-called slope zones [15–17]. Recharge zones located in the uppermost slope areas with a high sand content and infiltration capacity are declared to be vulnerable to nitrate pollution [18,19]. Conversely, discharge zones in the lowest parts of slopes with a lower capacity for infiltration and with groundwater approaching land surface or a surface water body can be waterlogged and their nitrate load denitrificated. Tile drainage was confirmed as another factor, which amplifies nitrate leaching to surface and subsurface waters [20,21]. Topsoil variability and hydraulic properties of the subsoil root zone (extending to one meter and deeper) are needed to estimate the risk of nitrate leaching and adopt relevant measures [7,22].

The field measurement of K_s and *FWC* is demanding and costly, especially when larger areas need to be covered. Likewise, the routine laboratory method, i.e., soil–water retention curve, developed from volumetric water content and water potential for deriving *FWC*, is difficult and time-consuming [23]. An alternative tool for finding *FWC* and K_s is the use of easy-to-measure soil properties via pedotransfer functions (PTFs). Rasoulzadeh and Fatemi [24] successfully tested the ROSETTA PTF to merge the diverse infiltration curves toward a single-scaled curve just with particle size distribution. Abdelbaki et al. [25] established good accuracy of many previously developed PTFs for predicting K_s using particle size distribution, bulk density, total porosity and organic matter content. Novotný et al. [26] developed PTFs of the *FWC* for the Czech Republic and Slovak Republic conditions. Similarly, Saxton and Rawls [23] developed new soil water characteristic equations from the currently available USDA soil database, using only the readily available soil texture and organic matter variables.

Spatial assessment of soil hydraulic properties is possible by direct measurements and subsequent interpolation of values. This approach assumes a continuous change in soil properties between points. Haberle et al. [27,28] show that soil properties can change abruptly, and consequently, the use of interpolation methods provides results with limited accuracy. A suitable approach for assessing soil hydraulic properties is offered by remote sensing (RS), which has considerable potential, especially for precision agriculture and, by extension, for protecting surface waters from eutrophication [29,30]. Although the spatial variability of soil hydraulic properties is very important, RS data have received relatively little attention in this field. Most studies focus mainly on the assessment of soil moisture or soil water content. Currently, a number of systems based on active and passive radar remote sensing and synthetic multisource datasets are available (see [31,32]). A major drawback of these data is the very small scale resolution, which is completely inadequate for assessing individual soil blocks. The use of high spatial resolution multispectral satellite data (e.g., Sentinel 2 and Landsat 8 OLI/TIRS) and very high resolution aerial and UAV

(unmanned aerial vehicle) data seems to be more appropriate. In particular, the use of hyperspectral [33,34] and thermal data [35–37] has great potential.

The use of optical spectral data is based on the assumption of a change in spectral reflectance as a function of the change in soil or vegetation canopy water content due to stand water stress. A detailed analysis of the spectral response of different soil types with various water infiltration rate was carried out by Francos et al. [33], showing good agreement between the spectral properties of the soil and the rate of water infiltration into the soil. The combination of Sentinel 2 satellite data and the OPTRAM (OPtical TRApezoid Model proposed by Sadeghi et al. [38]) model showed good agreement between spectral data and soil moisture [39]. Furthermore, Haberle et al. [27] found good results of *FWC* estimation, using an RGB index calculated from UAV multispectral data for crops affected by long-term water deficit.

The methods based on thermal data allow the assessment of thermodynamic changes of the vegetation and soil surface, depending on the change in water content and evaporation of water from the surface. The advantage of these methods is their high sensitivity to dynamic changes in the surface energy balance. Some approaches use thermal data, e.g., the evaporation test [37], evapotranspiration modelling [40], thermal-optical trapezoid model [41], estimation of volumetric moisture content based on thermal inertia method [35,36], and estimation of volumetric moisture content based on temperature rising rate vegetation dryness index—TRRVDI [42]. A common feature of these methods is the relatively complicated calculation of individual parameters involving other supplementary inputs, such as meteorological data.

Currently, we are witnessing a significant development of data analysis methods based on the principles of artificial intelligence (AI). These are advanced methods of machine learning (ML) or deep learning (DL). The ML methods are increasingly being used to assess qualitative and quantitative indicators of the Earth's surface through RS data [43]. These are various algorithms that can provide multivariate, nonlinear, nonparametric regression or classification [43]. The ML methods have the advantage of describing complex problems [44], such as the problem of assessing soil hydraulic properties using RS (see e.g., [45,46]).

This work aimed to use crop water stress, derived from thermal and hyperspectral aerial data, combined with ML for the spatial assessment of K_s and *FWC* at selected sites with different soil properties and vegetation cover. The specific aim is to discuss the possibilities of the approach used and its limitations.

2. Materials and Methods

2.1. Study Sites

The study sites were located in two regions in the Czech Republic with different soil and climate conditions, in the Bohemian–Moravian Highlands and the lower Jizera River (Figure 1). Both regions are not only agricultural areas, producing cereals and oilseed rape as well as vegetables, potatoes and silage maize, i.e., crops causing an increased risk of nitrate leaching [47], but also important zones of drinking water for more than a million people living in Prague and other locations.

The Bohemian–Moravian Highlands is a hilly area with slight to moderate sloping fields. The area belongs to the Švihov drinking water reservoir basin on the Želivka River, which is an important source of drinking water for a large part of the Czech Republic. The water quality in this reservoir is strongly influenced by water retention in the catchment and the transport of substances by surface and subsurface runoff from arable land [48].

Agricultural production is focused mostly on growing cereals, silage maize, oilseed rape, and potatoes. The local climate is classified as moderately warm, according to Quitt [49], with a mean annual precipitation of 721 mm and air temperature of 8.2 °C. The bedrock consists of partially migmatized paragneiss with mostly higher degrees of weathering [50].
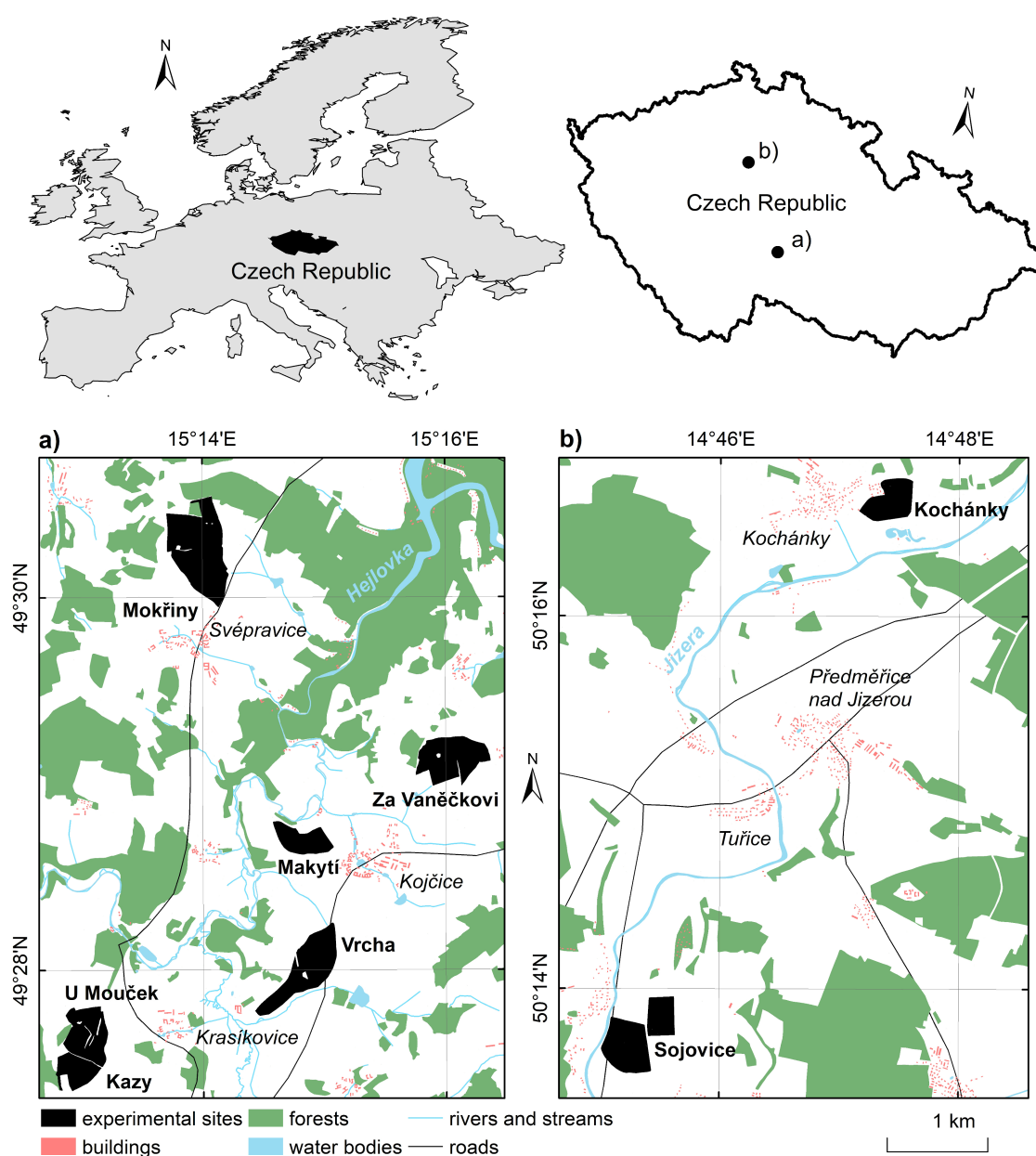
Figure 1. Area of interest with highlighted study sites.

The distribution of soil types (carried out by Research Institute for Soil and Water Conservation, Czech Republic) reflects the catchment slope zones, which are divided into recharge zones (the uppermost slope areas), and discharge zones (the lowest slope areas [51]). Both zones are bridged by transient zones located mainly in the middle sections of slopes. The dominant soil types of transient and recharge zones are Eutric/Dystric Cambisol and Eutric/Dystric Cambisol (Arenic) [52], which are texturally light (stony sandy loam or loamy sand), quite shallow and permeable (especially Eutric/Dystric Cambisol (Arenic)). Other shallow and permeable soils with coarse fragments can occur in the recharge zone (Leptic Cambisol and Cambic Leptosol). More clayey soils with higher moisture-holding capacity (e.g., Eutric/Dystric Stagnic Cambisol, Eutric/Dystric Stagnosol) are in the discharge and discharge/transient zones, with dominating medium-deep sandy loam and deep loams. See Table 1 for more details.

Six fields with heterogeneous soils were selected for the study. Crop cover was represented by winter wheat (*Triticum aestivum* L.), pea (*Pisum sativum* L.) and a silage

mixture (pea, spring wheat, red clover *Trifolium pratense* L.) during the RS campaigns. See Figure 1 and Table 2 for more details.

Table 1. Basic characteristics of the study sites and number of sampling points for saturated hydraulic conductivity of soil (K_s; cm·h^{-1}) and field water capacity (*FWC*; vol. %).

Locality	Soil Type [a]	Altitude (m a.s.l.)	Area (ha)	Slope (°)	Systematic Drainage (%)	Number of Samples K_s	FWC
Za Vaněčkovi	E/DC, E/DSC, E/DCA, E/DS	569	25.3	4.2	61	18	26 (21) [b]
Mokřiny	E/DC, LC, E/DSC, E/DS, CL	578	41.4	2.3	< 5	–	22
Makytí	E/DC	533	12.1	3.6	–	4	20
Vrcha	E/DC, LC, E/DSC, CL, E/DCA	514	26.9	4.6	–	–	23
U Mouček	E/DC	544	18.5	3.8	–	6	21
Kazy	E/DC, E/DCA, LC, CL, CA, LC	550	10.0	2.6	–	–	11
Kochánky	LFA, EFL, LRA, SRA, HP	230	15.7	1.4	–	5	21
Sojovice	LFA, EFL, SRA, LRA	221	36.9	1.1	–	–	35

[a] Note: E/DC—Eutric/Distric Cambisol, E/DSC—Eutric/Dystric Stagnic Cambisol, E/DCA—Eutric/Dystric Cambisol (Arenic), E/DS—Eutric/Dystric Stagnosol, LC—Leptic Cambisol, CL—Cambic Leptosol, CA—Cambisols, LFA—Leptic Fluvisol (Arenic), EFL—Eutric Fluvisol (Loamic), LRA—Leptic Regosol (Arenic), SRA—Skeletic Regosol (Arenic), HP—Haplic Phaeozems. [b] Note: The number of sampling points for a depth of 0.3–0.6 m.

Table 2. Overview of dates and times of aerial imaging and crop cover at individual study sites.

Locality	Date	Time (UTC) [a]	No. of Days after Rain > 1 mm	Crop	LAI
Za Vaněčkovi	2017 May 11	7:15	1	Winter wheat	2.46
	2017 May 28	9:50	6	Winter wheat	2.91
Mokřiny	2017 May 11	7:15	1	Winter wheat	2.73
	2017 May 28	9:50	6	Winter wheat	3.49
Makytí	2017 May 11	7:15	1	Pea	0.08
	2017 May 28	9:50	6	Pea	0.50
Vrcha	2018 May 27	7:10	4	Winter wheat	2.57
U Mouček	2018 May 27	7:10	4	Mixture for silage	3.74
Kazy	2018 May 27	7:10	4	Winter wheat	2.32
Kochánky	2018 May 29	7:30	6	Winter wheat	3.10
Sojovice	2018 May 29	7:30	6	Potatoes	3.23

[a] Note: The local daylight saving time is UTC+2.

The area along the lower Jizera River with the riverbank filtration system (Káraný waterworks) is the source of the remaining 25 % of the total drinking water supply for Prague. Water is extracted by over 500 bore wells regularly distributed along 22 km of the alluvium aquifer/river interface supplied by water seeping from the river and percolation from adjacent fields with a high nitrate content of 100–250 mg·l^{-1} [53]. The area is used for the cultivation of irrigated vegetables (radish, lettuce, carrot, broccoli, onion, garlic, celery, parsley, cabbage, kohlrabi, and red beet), and early and medium potatoes. Non-irrigated winter and spring wheat, barley, sugar beet, or maize are irregularly included in the vegetable sequence. Soils are represented mostly by light textured soils (loamy-sand and sandy-loam soils) with low water capacity and high spatial variability. The local climate is classified as warm, according to Quitt [49], with a mean annual precipitation of 573 mm and air temperature of 9.5 °C.

The area of interest is mainly built by marine sediments of the Bohemian Cretaceous Basin; the watercourse valleys are filled with Pleistocene (Quaternary) fluvial and alluvial sediments that have resulted in the high spatial variability of soil texture. Often, a sharp difference could be observed on the scale of only one to two meters. Several soil types [52]

were identified at the study sites: Eutric Fluvisol (Loamic), Leptic Fluvisol (Arenic), Leptic Regosol (Arenic), Skeletic Regosol (Arenic), and Haplic Phaeozems (see Figure 2 for spatial distribution). The texture ranged from loam to sandy loam and sandy soil with skeletons, especially in the subsoil. The spatial variability of soil types corresponds to the great variability of the moisture-holding capacity of the topsoil and subsoil [28]. The two experimental sites near the villages Sojovice (three field blocks) and Kochánky in the lower Jizera River region were monitored (Figure 1). Winter wheat was grown in the years of aerial data acquisition at the Kochánky site, and irrigated potatoes were grown on part of Sojovice field blocks.
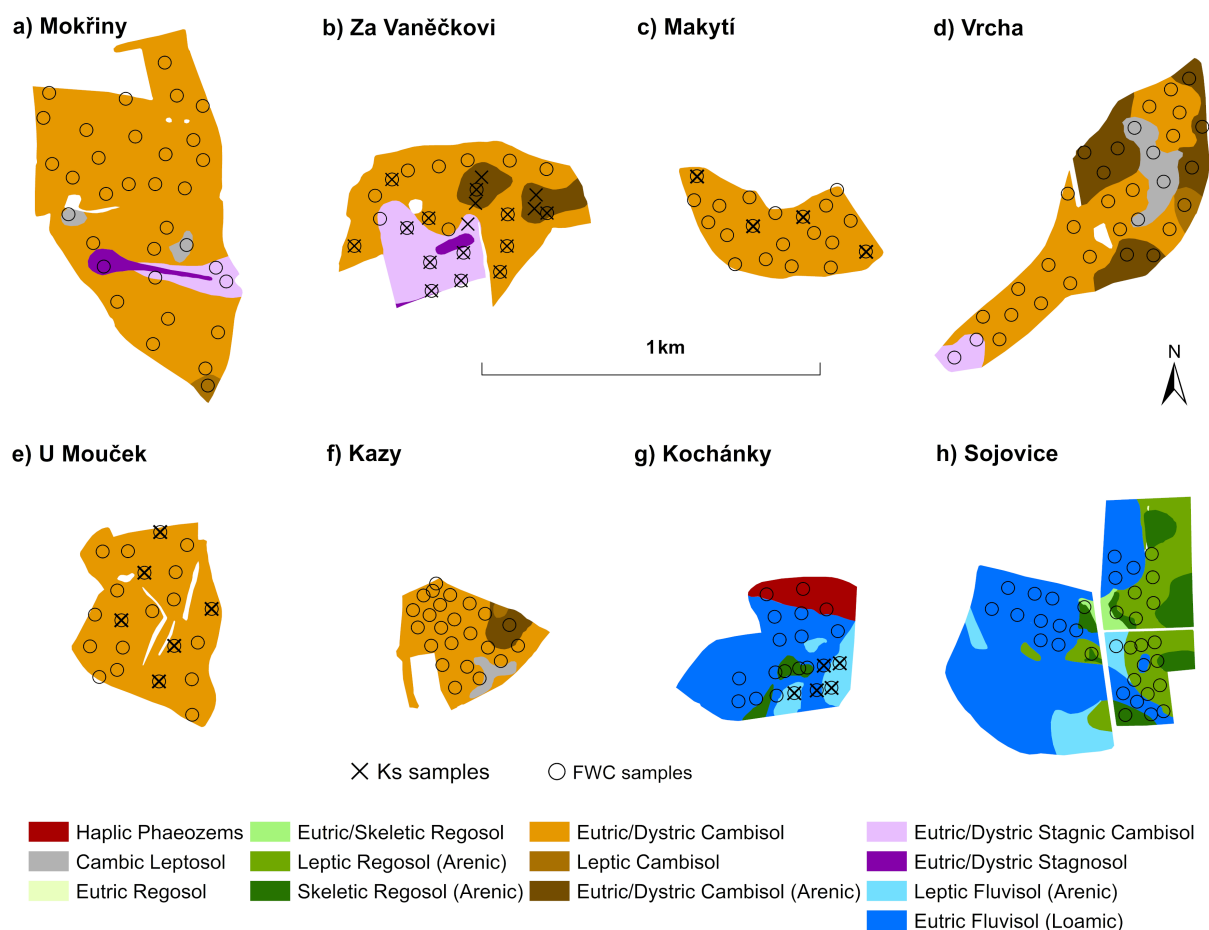

Figure 2. Spatial distribution of soil types within the study sites.

2.2. Measurements of Saturated Soil Hydraulic Conductivity and Determination of Field Water Capacity

Values of saturated soil hydraulic conductivity (K_s; cm·h^{-1}) were measured on the soil surface (after removing the top layer of about 3–5 cm) with three to six pressure infiltrometers designed by the Research Institute for Soil and Water Conservation (Czech Republic) at each measuring point. For further analysis, the median of the measured values was calculated for each point. Measuring points for K_s with different soil permeability and fertility were selected in the fields of Za Vaněčkovi, Makytí, U Mouček and Kochánky, which were measured after winter wheat or corn (*Zea mays* L.) harvests (Za Vaněčkovi 2017 and 2018), and when winter wheat was grown (Makytí, U Mouček and Kochánky in 2020).

Infiltrometers were based on the principle of Mariott's bottle and they were connected with an OMEGA OM-PL420 data logger. A capacitive sensor (CLM type with a rod electrode and reference tube) was used to measure the level change in the infiltrometer storage tank. The sensor is connected to the data logger and the logged data correspond directly to the values of the measured water level in the storage tank. The water level was

measured between the minimum and maximum levels, marked by lines on the body of the infiltrometer tank, every 20 seconds. Data evaluation was performed based on the two- and three parametric Philip's equations [54]. The K_s values from both equations were averaged.

To determine the *FWC* (the maximum amount of water that a particular soil can hold after drainage of the water contained in the macropores; vol. %), soil samples were taken from the topsoil (0–0.3 m) and subsoil (0.3–0.6 m) layers in all fields in Bohemian–Moravian Highlands and lower Jizera River (Table 1) and were analyzed for the particle size distribution by the pipette method [55]. A fine particle size fraction (F_p, %) <0.01 mm was used for calculating the *FWC* with a simple PTF [26]:

$$FWC = 6.66 + 1.03 \cdot F_p - 0.008 \cdot F_p{}^2 \tag{1}$$

The values of *FWC* were reduced, according to coarse fragments content (>2 mm).

2.3. Remote Sensing Data

Airborne hyperspectral optical and thermal data were used to analyze soil infiltration properties and *FWC*. Images were acquired using CASI-1500, SASI-600 and TASI-600 hyperspectral sensors (ITRES Ltd.). A summary of the dates and time of imaging at each site is shown in Table 2. All images were acquired in cloudless weather.

The aerial thermal images acquired with the TASI-600 thermal hyperspectral sensor were obtained with a spectral data resolution of 110 nm in the range of 8–11 μm. A total of 32 spectral bands were recorded. The spatial resolution was 5 m. The data were used to calculate the surface temperature layer. The aerial hyperspectral images obtained by the CASI-1500 optical hyperspectral scanner were taken with a spectral resolution of 10 nm data in the range 380–1050 nm. A total of 72 spectral bands were recorded. The spatial resolution ranged from 2 m to 2.5 m depending on the imaging date. For analyses, the data were resampled to a resolution of 5 m. Using a SASI-600 optical hyperspectral scanner, images were acquired with a spectral resolution of 15 nm data in the range 950–2450 nm. A total of 100 spectral bands were recorded. The data were acquired at a spatial resolution of 5 m. All the aerial data were provided by the Global Change Research Institute, Czech Academy of Science (CzechGlobe) at the L2 processing level. The data provider performed all the necessary geometric and radiometric corrections of the data (for more details see https://olc.czechglobe.cz/en/main-page/, accessed on 20 May 2021).

The digital terrain model (DMT), the height of the crop cover and the meteorological data were used as additional data for the calculation of individual variables.

The digital terrain model and digital surface model (DMS) were created from LiDAR data acquired for all the areas of interest during the aerial campaigns. A Riegl LMS Q780 sensor with a spatial resolution of 0.5 points per square meter was used for imaging. The data were provided by CzechGlobe again. The DMT and DMS were obtained with the LasTools (https://rapidlasso.com/lastools/, accessed on 20 May 2021), using the lascanopy tool. The DMT was created by filtering the point cloud values to the 1% quantile level of the individual point values with a resolution of 5 × 5 m. The DMS was created using a 99% quantile filter for 5 × 5 m resolution. The height of crop cover was determined as the difference between the DMS and DMT. The DMT and crop cover height layers were used to calculate energy fluxes and crop water stress index.

Meteorological data (air temperature and relative humidity at 2 m, global radiation and air velocity at 2 m) were measured at the areas of interest, using automatic weather stations. The air temperature layer in the area of interest was calculated based on the assumption of an adiabatic surface temperature change of 0.65 °C per 100 m of altitude, using the DMT and the measured air temperature value by the automatic weather station. The wind speed was assumed to be spatially constant for each site.

The estimation of K_s and *FWC* was based on the assumption of a relationship between the hydraulic soil properties and the expression of crop water stress. Crop water stress can be identified using the so-called crop water stress index (CWSI; [56,57]), which is based

on the assumption of a change in the surface energy balance. The CWSI index attempts to relativize this change in relation to the ability of the environment to accept water vapor. The CWSI index was calculated as follows [56]:

$$CWSI = 1 - \frac{\Delta + \gamma^*}{\Delta + \gamma\left(1 + \frac{r_c}{r_a}\right)},$$ (2)

where Δ is the slope of the temperature gradient with respect to the moisture gradient (K·kPa^{-1}), γ is the psychrometric constant (kPa·K^{-1}), r_c represents the resistance of the vegetation to water vapor transfer (s·m^{-1}), and r_a is the aerodynamic resistance of the surface to heat and momentum transfer (s·m^{-1}). The γ^* is the modified psychrometric constant (kPa·K^{-1}) calculated using the following formula [56]:

$$\gamma^* = \gamma\left(1 + \frac{r_{cp}}{r_a}\right),$$ (3)

where r_{cp} is the resistance of the vegetation to water vapor transport under conditions of potential evaporation from the surface (s·m^{-1}).

The calculation of the aerodynamic surface resistance for heat and momentum transfer r_a is based on the Monin–Obukhov theory of similarity [58,59] with respect to the aerodynamic surface roughness [60]. The aerodynamic resistance of the surface was calculated based on the following relation [61]:

$$r_a = \frac{\left[\ln\left(\frac{z-d}{z_{0m}}\right) - \Psi_m(\varsigma)\right]\left[\ln\left(\frac{z-d}{z_{0h}}\right) - \Psi_h(\varsigma)\right]}{U \cdot \kappa^2},$$ (4)

where z is the height above the surface corresponding to the mixing layer; d is the effective height of the vegetation (m); z_{0m} and z_{0h} are the aerodynamic roughness of the vegetation for the transfer of water vapor, heat and momentum; U is the wind speed converted, according to the logarithmic law for the height z (m·s^{-1}); and κ is the Kármán constant. The values of $\Psi_h(\varsigma)$ and $\Psi_m(\varsigma)$ are the stability coefficients for heat and momentum transfer in the atmospheric boundary layer calculated as a function of its stability [62]. The individual parameters of the equation were calculated by an iterative procedure given by Brutsaert [63].

The surface resistance value for water vapour transfer r_c was calculated using the following formula:

$$r_c = \left[\left(\frac{\Delta + \gamma}{\Omega} - \Delta\right)\frac{1}{\gamma} - 1\right]r_a,$$ (5)

where Ω is the so-called decoupling coefficient or also the relative evaporation (rel., [64]). The value of r_{cp} (s·m^{-1}) was derived from the assumption that r_{cp} is equal to r_c for potential evaporation. In this case, the value of r_{cp} can be calculated using the following formula:

$$r_{cp} = \frac{(E_s - e_a)\rho c_p}{\gamma \cdot LE_p} - r_a,$$ (6)

where E_s is the saturated water vapor pressure at stand level (kPa), e_a is the air water vapor pressure (kPa), and LE_p is the latent heat flux of evaporation for potential evaporation (W·m^{-2}, [56]).

Because the expected more rapid development of crop water stress in areas with higher infiltration ability affects crop cover development, we used the spectral vegetation index MSAVI (modified soil adjusted vegetation index; [65]) as an additional variable to estimate K_s and FWC calculated according to the following equation:

$$MSAVI = 0.5 \cdot \left(2R_{NIR} + 1 - \sqrt{(2R_{NIR} + 1)^2 - 8(R_{NIR} - R_{RED})}\right).$$ (7)

The MSAVI index is significantly correlated with the vegetation production characteristics, such as canopy height [66], leaf area index and aboveground biomass amount [65]. The surface moisture can vary significantly among dates and sites, and for this reason, we used the normalized difference moisture index (NDMI; [67]), which is significantly correlated with surface moisture, as an additional variable to estimate the *FWC*. The *NDMI* was calculated using the following relationship:

$$NDMI = \frac{R_{NIR} - R_{SWIR}}{R_{NIR} + R_{SWIR}}, \tag{8}$$

where R_{band} is a spectral reflectance (rel.) in particular spectral band. The spectral bands selected for this study were 670 nm (red band; RED), 860 nm (near infrared band; NIR) and 1610 nm (shortwave infrared band; SWIR). The wavelength used for the red band corresponds to a spectral region that is essentially insensitive to chlorophyll *a* content [68]. The magnitude of reflectance in the NIR spectral domain is governed by structural discontinuities encountered in the leaf and plants, and spectral reflectance in the SWIR domain is related especially to water absorption [69]. In our case, the selection of spectral bands with the wavelength in 670, 860 and 1610 nm corresponds closely to central wavelengths of the Sentinel 2 MSI and Landsat 8 OLI satellite bands. See https://sentinels.copernicus.eu/web/sentinel/technical-guides/sentinel-2-msi/msi-instrument (accessed on 20 May 2021) and https://landsat.gsfc.nasa.gov/landsat-8/landsat-8-overview (accessed on 20 May 2021) for more details.

The leaf area index (LAI, m$^2 \cdot$m^{-2}) was calculated as a proxy value for each study site based on the following relationship [70]:

$$LAI = \frac{LAI_1 + LAI_2}{2}, \tag{9}$$

where

$$LAI_1 = \begin{cases} 11 \cdot SAVI^3 & SAVI > 0; \ SAVI \leq 0.817 \\ 6 & SAVI > 0.817 \end{cases} \tag{10}$$

and

$$LAI_2 = \begin{cases} -\dfrac{\ln \frac{0.61 - SAVI}{0.51}}{0.91} & SAVI > 0; \ SAVI \leq 0.61 \\ 6 & SAVI > 0.61 \end{cases} \tag{11}$$

SAVI is the soil adjusted vegetation index [71]:

$$SAVI = \frac{(1 + L) \cdot (R_{NIR} - R_{RED})}{L + R_{NIR} + R_{RED}}, \tag{12}$$

where *L* is a constant (*L* = 0.5). The LAI was measured directly using Plant Canopy Meter Li-2000 (Li-COR, Ltd.) at the study sites of Za Vaněčkovi, Mokřiny, Kazy and Vrcha for each sampling point on the date of aerial data acquisition. The mean values of LAI were used for these sites (see Table 1). The MSAVI and SAVI spectral indices were calculated from the CASI-1500 data; the NDMI spectral index was calculated from the CASI-1500 and SASI-600 data.

The SEBCS for QGIS [72] was used for the calculation of the variables.

The MSAVI, NDMI and CWSI index values were extracted for each sampling point, using zonal statistics calculation. For each point, median values were calculated for a circle with a radius of 5 m. The reason for using the median was to limit the impact of outliers in the source data.

2.4. K_s and FWC Estimation from Aerial Data

The estimation of the spatial distribution of K_s and *FWC* is based on the assumption of the relationship between the observed characteristics and the expression of stand water stress. Our hypothesis was that areas with higher infiltration rate will develop water stress

earlier than areas with a lower infiltration rate. In this case, the *FWC* is an indirect indicator of soil infiltration capacity. Here, we assume that soils with greater skeleton content, and therefore lower *FWC*, will exhibit greater infiltration capacity.

A nonlinear model based on the machine learning method of support vector regression (SVR; [73,74]) was used to estimate the K_s and *FWC* at the study sites. The SVR method was used, due to the assumption of a nonlinear relationship between the variables. The e1071 package [75] in the R platform for statistical computing [76] was used for model building.

The radial basis kernel (RBF) was used for the SVR model. The model was tuned with a variable insensitive-loss function epsilon in the range of 0 to 1.0 with step 0.1 and with the cost of constraints violation in the range 2^2 to 2^9 with step 2^{n+1}, where n is an exponent from the previous calculation step. The gamma parameter was set as 1/number of values in the dataset. See the e1071 package documentation [75] for more details. The best model was chosen for the prediction of the estimated data based on spectral indices CWSI, MSAVI and NDMI.

The estimated values of K_s and *FWC* using the SVR model were related to the measured data, using a linear regression method. The bias of the estimated values was calculated using the root mean square error (RMSE) according to the following equation:

$$RMSE = \sqrt{\frac{1}{n} \sum_{i=1}^{n} (P_i - O_i)^2}, \tag{13}$$

where n is a number of values in the dataset, P_i is the predicted data, and O_i is the observed data.

2.5. Statistical Analysis

The statistical analysis was performed to compare the K_s and *FWC* values and *FWC* values measured in two different soil profiles at the study sites. A simple linear regression method was used for the evaluation. The normality of the data was tested, using the Shapiro–Wilk test.

Comparison of the K_s and *FWC* field values with the results estimated from aerial data was performed, using the simple linear regression method.

All statistical tests were performed in R platform for statistical computing [76] at the probability level of $\alpha = 5\%$.

3. Results

3.1. Measured Data of K_s and *FWC*

The measured values of K_s and *FWC* showed considerable variability depending on the soil conditions of the study sites. The *FWC* values also varied between the monitored topsoil and subsoil. Values of K_s ranged from 2.5 to nearly 49 cm·h^{-1} at each site. While predominantly low K_s values were observed at the Za Vaněčkovi site ($\bar{x} = 10.5$, sd = 8.5), a wide range of values, including high values ($\bar{x} = 23.5$, sd = 16.2), was observed in the variable soils of the Kochánky site (deep loamy humic vs. shallow sandy and skeletal). At the U Mouček and Makytí sites, the mean K_s values were 14.5 and 18.8 with a standard deviation of 4.9 and 8.3, respectively. An overview of the distribution of K_s values is shown in Figure 3a).

The highest mean *FWC* values with high variability for topsoil were found at the sites in the lower Jizera River areas ($\bar{x} = 27.0$, sd = 7.2 and $\bar{x} = 25.8$, sd = 4.7 for Kochánky and Sojovice, respectively). In contrast, low *FWC* values were recorded at the sites in the Bohemian–Moravian Highlands. Except for the site Za Vaněčkovi ($\bar{x} = 25.6$, sd = 3.2) with high soil variability and systematic drainage, here, the *FWC* values for topsoil had rather less variance. A summary of the distribution of values is shown in Figure 3b). The *FWC* values for the subsoil layer were lower than those for the topsoil layer, given some soils' greater skeletal or sand content. The values were again higher in the Lower Jizera River

area than in the Bohemian–Moravian Highlands. An overview of the distribution of values is shown in Figure 3b).
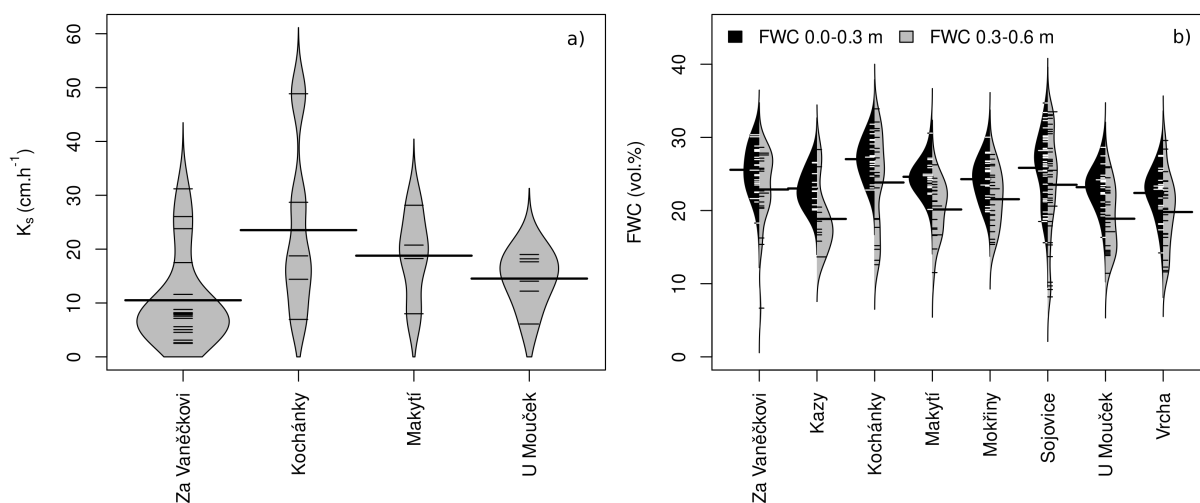

Figure 3. Summary of the distribution of values of (**a**) saturated soil hydraulic capacity (K_s) and (**b**) field water capacity (*FWC*) measured at the study sites. The short horizontal lines indicate the measured values; the long horizontal line indicates the arithmetic mean of the values.

An inverse relationship is expected between K_s and *FWC*, i.e., the lower the *FWC*, the higher the water infiltration rate into the soil. The analysis of the relationship between K_s and *FWC* for topsoil confirmed a significant relationship between the two variables; however, the relationship showed a low level of correlation ($R^2 = 0.17$, $F_{1,31} = 6.4$, $p < 0.05$). The relationship between the K_s and *FWC* was not significant for the subsoil layer or the whole soil profile studied. The logarithmic transformation of the data was used because the K_s values did not show a normal distribution (Shapiro–Wilk test: $W = 0.87$, $p < 0.05$). The resulting relationship is shown in Figure 4a).
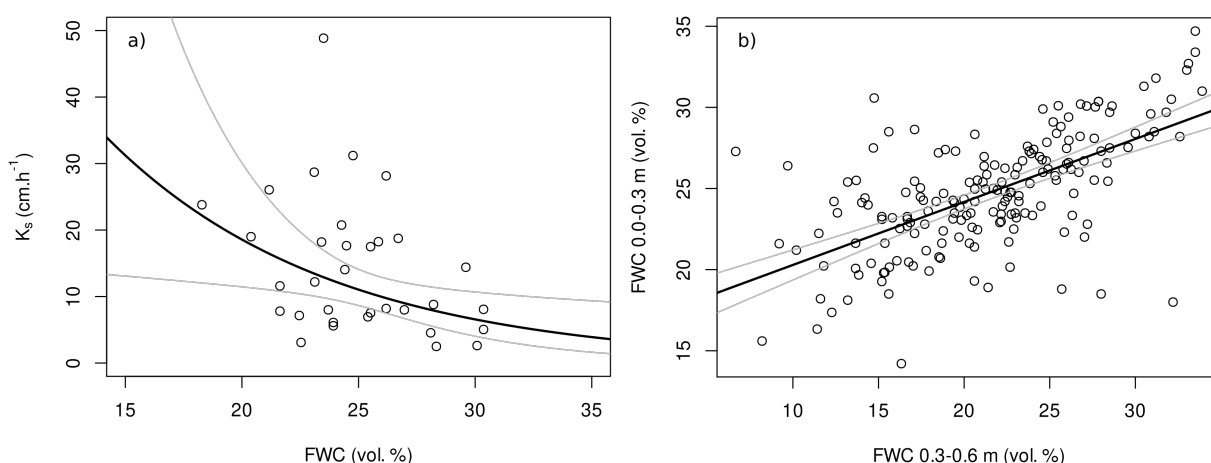

Figure 4. Relationship between (**a**) field water capacity (*FWC*, vol. %) for topsoil and saturated soil hydraulic conductivity (K_s, cm·h^{-1}), and (**b**) between *FWC* (vol. %) of subsoil (0.3 to 0.6 m) and topsoil (0 to 0.3 m). The 95% confidence interval is marked by grey lines.

Analysis of the relationship between the *FWC* values measured in the topsoil (0–0.3 m) and subsoil (0.3–0.6 m) showed a significant regression relationship ($R^2 = 0.38$, $F_{1,180} = 112.6$, $p < 0.05$), shown in Figure 4b).

3.2. Estimation of K_s and FWC Data from Aerial Imaging

The analysis of the relationship between the measured and modelled K_s values based on the aerial data for the site of Za Vaněčkovi showed that the regression coefficient value was only $R^2 = 0.46$ ($F_{1,16} = 13.4$, $p < 0.05$, RMSE = 6.62) for the imaging term of 11 May 2017, compared to the high value of $R^2 = 0.96$ on 28 May 2017 ($F_{1,16} = 402.8$, $p < 0.05$, RMSE = 1.61). The reason for the difference between the two dates was the different saturation of the soil profile, and therefore, the root zone of the stands, with water at the time of imaging (see below). Because the assumption of stand water stress development was not met for 11 May 2017, these data were excluded from a further K_s analysis. The regression relationship was not calculated separately for the other sites, due to the low number of measurements. However, the combination of data from the Za Vaněčkovi, U Mouček, Makytí and Kochánky sites showed good agreement between measured and estimated data ($R^2 = 0.77$, $F_{1,31} = 103.8$, $p < 0.05$, RMSE = 4.95). The regression relationship is shown in Figure 5.
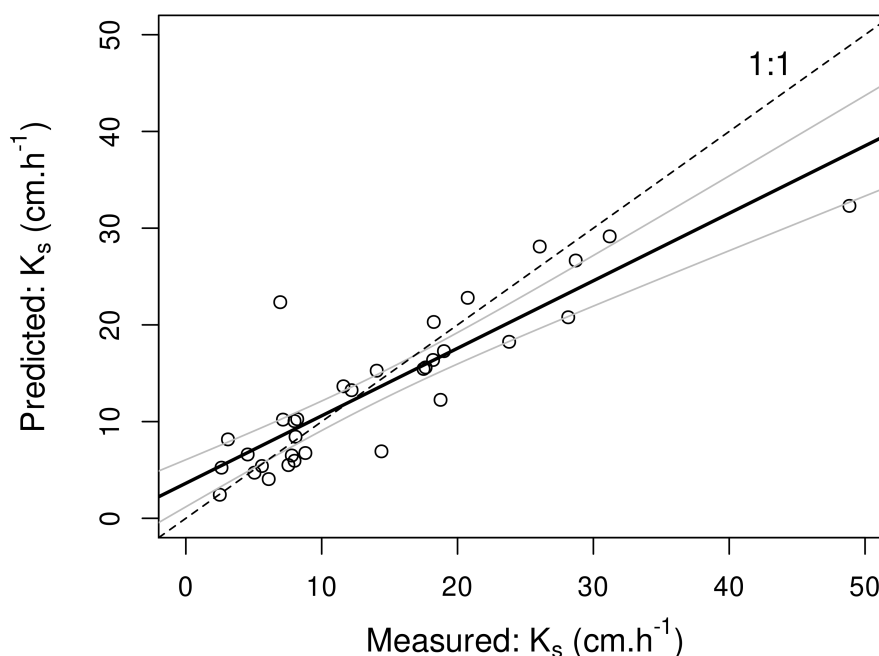

Figure 5. Relationship between measured and predicted data of saturated soil hydraulic conductivity (K_s, cm·h^{-1}) by the SVR model based on aerial data. The 95% confidence interval is marked by grey lines.

The regression coefficient values for the relationship between the measured *FWC* values for the soil depth of 0–0.3 m and the aerial data varied considerably between the sites. The regression coefficient values ranged from 0.38 to 0.99. Low regression coefficient values were obtained for the aerial data from 11 May 2017. The exception here was the Makytí site, which showed high regression coefficient values in 2017 for both observed dates ($R^2 = 0.99$ and $R^2 = 0.97$). In 2018, low values of R^2 were found for irrigated potato at the Sojovice site ($R^2 = 0.42$), for winter wheat crop at the Kochánky site ($R^2 = 0.43$) and for the U Mouček site ($R^2 = 0.38$), where the crop consisted of a cereal–leguminous mixture for silage. The values of the regression coefficient were around 0.8 at the sites Vrcha and Kazy. A detailed overview of the values is shown in Table 3 and in Figure 6a).
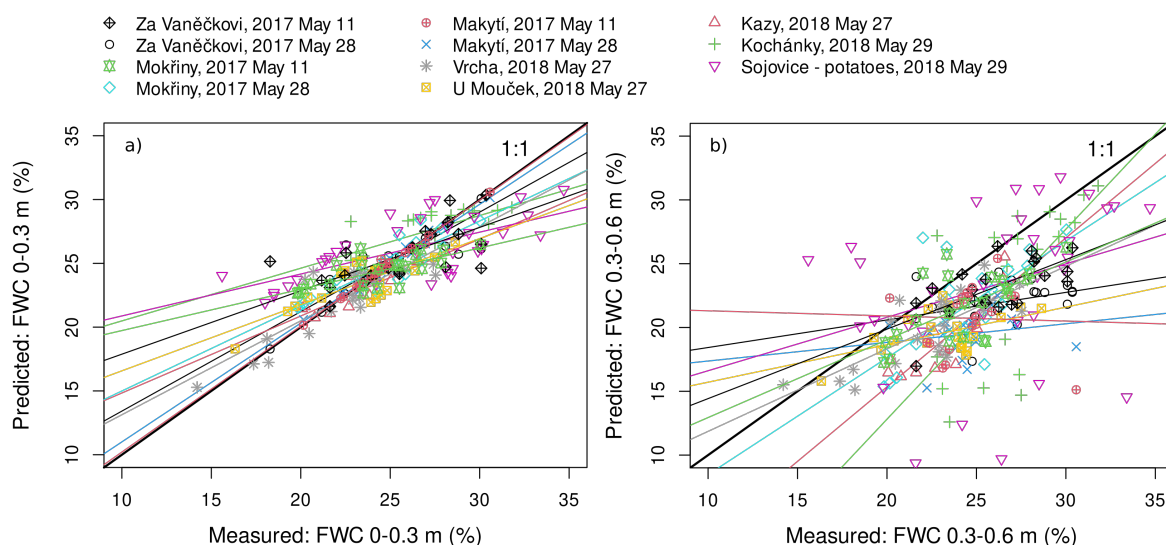
Figure 6. Regression relationship between measured and predicted data of field water capacity (*FWC*, %) for topsoil (**a**) and subsoil layer (**b**) for each study sites. Statistical description of the results is given in Tables 3 and 4.

The regression coefficient values for comparing the measured *FWC* values and the aerial data for the subsoil show a different character. Low values of R^2 remain for 11 May 2017, for the sites Za Vaněčkovi ($R^2 = 0.35$) and Makytí ($R^2 = 0.46$). In contrast, a strong relationship was found for the Mokřiny site ($R^2 = 0.81$). Low regression coefficients were also found for irrigated potatoes at the Sojovice site ($R^2 = 0.43$) and Za Vaněčkovi and Makytí sites ($R^2 = 0.12$ and 0.36, respectively) for the date of 28 May 2017. In the case of the Za Vaněčkovi site, the result is even inconclusive. Low values of the regression coefficient were also found for the sites U Mouček ($R^2 = 0.36$) and Vrcha ($R^2 = 0.50$). High values of the regression coefficient were found for the Mokřiny site for both imaging dates ($R^2 = 0.81$ for 11 May 2017 and even $R^2 = 0.99$ for 28 May 2017, respectively) and at the Kazy ($R^2 = 0.81$) and Kochánky ($R^2 = 0.84$) sites. The RMSE values are higher than for topsoil in most cases. A summary of the results comparing measured and estimated *FWC* values for the 0.3–0.6 m soil layer is shown in Table 4 and in Figure 6b).

Table 3. Results of regression analyses of the relationship between the modeled and measured values of topsoil field water capacity (*FWC*; vol. %) for particular study sites, dates of aerial data acquisition and crops.

Locality	Date	Crop	R^2	F	df	*p*-Level [a]	RMSE
Za Vaněčkovi	11 May 2017	Winter wheat	0.49	23.47	24	***	2.25
	28 May 2017	Winter wheat	0.80	98.20	24	***	1.41
Mokřiny	11May 2017	Winter wheat	0.52	21.44	20	***	2.06
	28 May 2017	Winter wheat	0.82	91.25	20	***	1.25
Makytí	11 May 2017	Pea	0.99	1609.0	18	***	0.22
	28 May 2017	Pea	0.97	498.20	18	***	0.40
Vrcha	27 May 2018	Winter wheat	0.83	102.60	21	***	1.31
U Mouček	27 May 2018	Mixture for silage	0.38	11.45	19	**	2.17
Kazy	27 May 2018	Winter wheat	0.78	31.06	9	***	1.17
Kochánky	29 May 2018	Winter wheat	0.43	14.05	19	***	2.04
Sojovice	29 May 2018	Potatoes	0.42	24.06	33	***	3.81

[a] Note: ***–$p < 0.001$, **–$p < 0.01$, *–$p < 0.05$, .–$p < 0.1$, n.s.–not significant.

Examples of the graphical output computed from the above models for K_s and *FWC* are shown in Figure 7. The image shows that both K_s and *FWC* varied considerably at the sites. In the Bohemian–Moravian Uplands, the study sites are very heterogeneous,

representing areas with increased infiltration capacity, mainly in the upland parts and in areas with shallow soil. In contrast, the soils in the lower Jizera area are composed of the fluvial and alluvial sediments with different skeleton content. The distribution of the modeled values largely corresponds to the delineation of soil types (Figure 2), but the spatial variability of soils is expressed at a more detailed scale.

Table 4. Results of regression analyses of the relationship between modeled and measured values of bottom soil layer field water capacity (*FWC*; vol. %) for particular study sites, dates of aerial data acquisition and crops.

Locality	Date	Crop	R^2	F	df	*p*-Level [a]	RMSE
Za Vaněčkovi	2017 May 11	Winter wheat	0.35	10.26	19	**	4.31
	2017 May 28	Winter wheat	0.12	2.71	19	n.s.	4.95
Mokřiny	2017 May 11	Winter wheat	0.81	85.78	20	***	1.75
	2017 May 28	Winter wheat	0.99	1996.0	20	***	0.37
Makytí	2017 May 11	Pea	0.46	15.34	18	**	2.72
	2017 May 28	Pea	0.36	10.59	18	**	3.64
Vrcha	2018 May 27	Winter wheat	0.50	21.01	21	***	3.56
U Mouček	2018 May 27	Mixture for silage	0.36	10.59	19	**	3.64
Kazy	2018 May 27	Winter wheat	0.81	37.19	9	***	2.19
Kochánky	2018 May 29	Winter wheat	0.84	95.37	19	***	2.66
Sojovice	2018 May 29	Potatoes	0.43	24.63	33	***	5.89

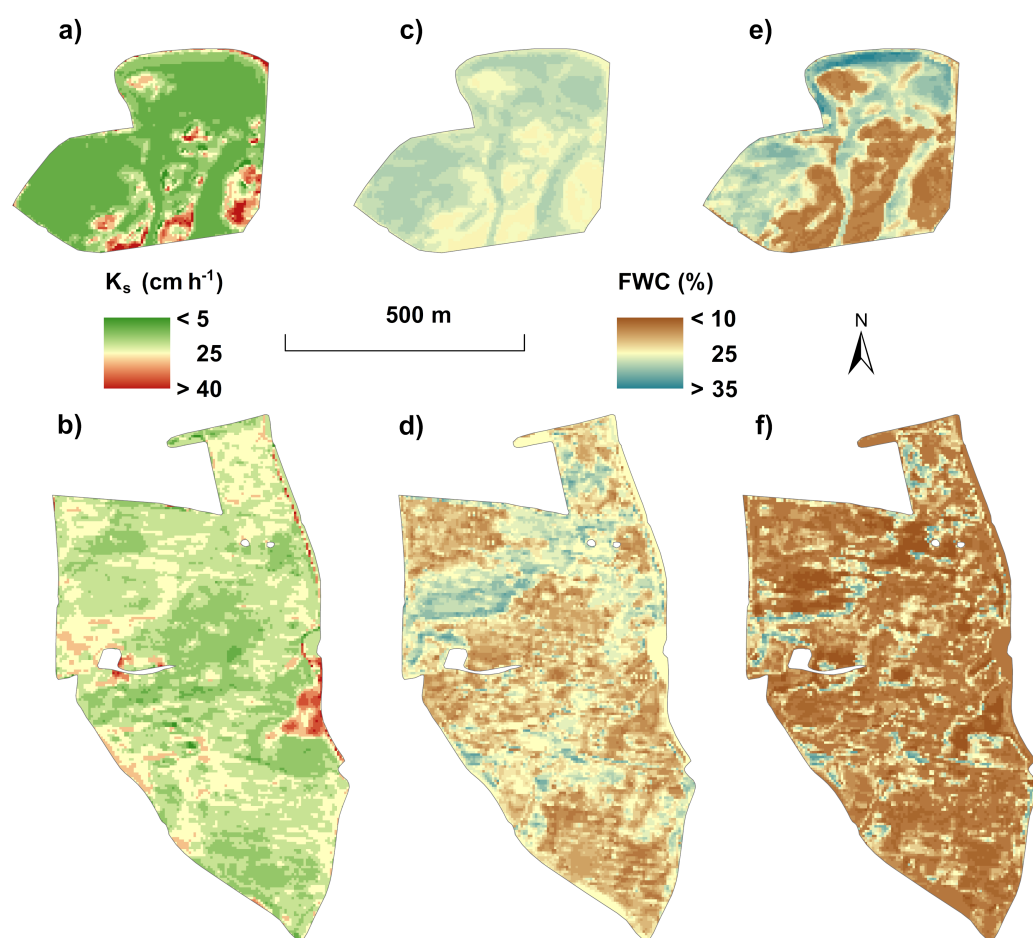[a] Note: ***–$p < 0.001$, **–$p < 0.01$, *–$p < 0.05$, .–$p < 0.1$, n.s.–not significant.

Figure 7. An example of spatial distribution of (**a**,**b**) saturated soil hydraulic conductivity (K_s, cm·h^{-1}) and field water capacity (*FWC*, %) for topsoil (**c**,**d**) and bottom soil layer (**e**,**f**) calculated by the SVR model based on aerial data.

The *FWC* images for the two depths studied show a similar pattern to the K_s outputs. However, the values are inverse; low *FWC* values correspond to elevated K_s values and vice versa. The *FWC* values in both the topsoil and subsoil show a similar spatial distribution; however, some differences are evident. As can be seen from the example for the Kochánky site (Figure 7c,e), the spatial differences of values are in some cases smaller in the topsoil layer. In contrast, larger differences of *FWC* in the field blocks are evident in the subsoil. It should be noted that the observed differences are site specific, e.g., there is a higher variability of values in the topsoil at the Vrcha site.

4. Discussion

The presented approach shows a relatively simple way of evaluating the spatial variability of hydraulic properties of soils, using remote sensing data usable in practice. However, the quality of the evaluation and estimation depends on several factors.

4.1. Data and Their Quality

The crucial factor is the quality of the data used to calibrate the proposed models. In this work, two different approaches were used to evaluate the hydraulic properties of soils in situ. A direct measurement was used for the K_s, and estimation of *FWC* was based on a simple PTF for soil hydrolimits (water content defined for specific values of water potentials). The K_s is an indicator of the infiltration capacity of the soil, respectively, the upper limit of the rate of water infiltration into the soil [77]. The infiltration rate is an essential property of the soil that has a clear connection with the manifestations of plant water stress, the amount of leached nitrates, or other nutrients from agricultural (including tile-drained) soils, and with an intensity of water erosion [78–80]. The problem of the practical use of direct in situ measurement of the K_s is technical, time, management and financial complexity. The accuracy of the K_s measurement is disputable, due to the impact of several factors affecting the measurement, e.g., spatially heterogeneous occurrence of preferential pathways (via macropores, cracks and fissures) significantly affected by previous soil moisture and biological activity (biopores), concentrated runoff pathways, local soil heterogeneity of skeletal content, organic matter and porosity, agrotechnical treatment (soil tillage) and also the compaction of subsoil due to the agricultural machinery [81–83].

The use of the *FWC* represents, in comparison with the determination of the K_s, a relatively more straightforward approach for the evaluation of hydraulic properties of soils. The determination of the *FWC* based on the PTF derived from the content of clay particles shows good agreement with the direct measurement of the *FWC* based on the measurement of soil moisture and soil water potential for several soil types [26]. However, the quality of the *FWC* estimate is also affected by the above effects. The method of using the PTF was successfully used, for example, by Haberle et al. [27] for the relationships between soil spatial variability and crop growth influenced by soil water stress.

The indirect proportion between the K_s and *FWC* is based on the assumption that skeletal and sandy soils with high non-capillary porosity have a lower level of *FWC* and, at the same time, a higher ability to infiltrate water into the soil profile, compared to heavier and more compacted soils [84,85]. With the increasing content of sand, skeleton and stones, the ability of the soil to retain water decreases during rainfall events, the soil profile quickly saturates with water (especially by the presence of macropores and biopores), and water drains away by shallow subsurface runoff [86,87]. Although the relationship found between the K_s and *FWC* for the topsoil layer shows an expected trend, the observed dependence between the variables is weak (see Figure 4a)). This result may be due to the above effect of local soil heterogeneity, in particular, a change in pore structure and preferential flow, which causes a significant variance of the K_s values (incl. extreme values) for a relatively small *FWC* range (see Figure 4a), [88]). As shown by Haberle et al. [28] for the lower Jizera river area, soil vulnerability to leaching given by texture (loamy-sand and sandy-loam soil) and the resulting low water capacity is amplified by high spatial

variability of soil properties, which is often manifested visually by water stress impacts, when non-irrigated crops are grown in the area.

The differences between the hydropedological properties of both areas and the topsoil and subsoil layer are mainly due to the soil profile's pedogenesis. In the area of the Bohemian–Moravian Highlands, there are various soil types with medium to high K_s and lower *FWC*. This is related to the fact that the topsoil water-retaining layer (a horizon) is relatively shallow (max. 30–40 cm), with a low to medium humus content, lighter in grain size distribution with a skeleton content of 2–10 %, which grows into the subsoil (up to 30 %), thereby reducing the *FWC*. The decrease in the K_s of some parts of the upper horizons of the Za Vaněčkovi, Mokřiny and Vrcha localities was due to the relief, the texturally heavier substrate and periodically stagnant water, which led to the formation of the Eutric/Dystric Stagnic Cambisol or Eutric/Dystric Stagnosol with an impermeable subsoil K_s [89]. The infiltration capacity of the soil is also limited by the mica content in the Mokřiny locality. Disruption of the soil profile in the locality Za Vaněčkovi is a significant factor due to artificial mixing during the tile drainage building in 1977. Collection and conduit drains were installed at depths of 1.0 m and 1.1 m, respectively, and the spacing of collection drains was 13 m or 20 m apart [18,90].

The situation is different in the area of the lower Jizera river. The local soils were created by alluvial activity based on sediment loads with diverse structure, while the deposition of individual layers can be very variable [53,91]. Therefore, there are soils with strongly different properties, and consequently, the K_s and *FWC* range is wider than in the Bohemian–Moravian Highlands (Figure 3). There are soils that are very deep, humus rich, on loess or river sediments, without skeleton, with a high *FWC* and medium K_s (Eutric Fluvisol (Loamic) and Haplic Phaeozem); texturally light, dry, humus-rich soils on sandy river terraces with a low skeleton content (Leptic Fluvisol (Arenic); and soils that are very shallow (dry), with low humus content on gravelly-sandy fluvial terraces with low *FWC* and high K_s (Leptic Regosol (Arenic) and Skeletic Regosol (Arenic)). The presence of organic alluvial sediments in the Eutric Fluvisol (Loamic) subsoil reduced the *FWC* differences between the topsoil and subsoil. In the case of both areas, soil tillage is also important, such as the temporary homogenization of the surface by plowing and the different compaction of the subsoil by the travel of agricultural machinery.

The quality of aerial data is also a major problem for evaluating the area distribution of the K_s and *FWC*. Although complex preprocessing is performed on the data by the provider, various random errors and inaccuracies can occur, especially for thermal data. The median of the values for a circular segment with a radius of 5 m was calculated to reduce the effect of random errors and extreme values for each sampled site. Although random errors in the RS data are problematic, the imaging date and time are much more significant. The degree of plant water stress development is a fundamental prerequisite for evaluating soil hydraulic properties of the locality. Here, it is important to choose a term that ensures reduced water availability in the soil for plants, i.e., preferably a few days after the last major atmospheric precipitation. As the overview in Table 3 shows, the resulting model of the *FWC* estimate for the topsoil is much better for 28 May 2017 (Za Vaněčkovi and Mokřiny sites), which was characterized by significantly lower availability of soil water for plants, compared to 11 May 2017. In the previous 14 day period, the total precipitation period was 9 mm, compared to 31 mm before the first date, with one day after the last precipitation for the first date and six days for the second (see Table 2). Due to the strong development of water stress of crops, there was a perfect agreement between the model and the measured data on 27 May 2018 (localities Vrcha, Kazy), when the sum of precipitation from 1 April 2018 to 26 May 2018 was only 30 mm, four days after the last precipitation (see Table 2). The use of irrigation systems that mask the hydropedological properties of soils is problematic in this regard; see, for example, the Sojovice locality (see Table 3). The reason for the worse *FWC* estimate in the topsoil layer in Kochánky was probably a sudden spatial change (in the order of 1–2 m; see [28]) of soil hydraulic properties and thus the

impact of water stress on vegetation. The effects of drought here were mainly influenced by subsoil, as confirmed by the high R^2 values (see Table 4 and Figure 6b)).

The choice of imaging time is also important for evaluating crop water stress as one of the indicators of soil hydraulic properties. Too early imaging can be affected by dew occurrence. Dew trapped on the vegetation canopy can mask the manifestation of water stress (wet surface), and directly saturates the water needs of the stand [92]. Dew may also impact transpiration suppression due to the increased leaf wetness duration (especially plants with larger leaves) and the decreased leaf temperature [93]. Vuollekoski et al. [94] showed a potential for large-scale dew harvesting (yearly cumulative yield as high as 100 l· m^2) in water-stressed areas (e.g., coastal regions of northern Africa and the Arabian Peninsula). The effect of evaporation of interception water (primarily in the upper leaves of the plants) is also significant, the intensity of which largely depends on the exposure of individual parts of soil blocks [93]. This problem is significant in temperate and probably also in tropical areas [95,96]. In most cases, the available time for aerial imaging is significantly limited by cumulus clouds forming in the morning and at noon. These are mainly the months when the vegetation cover reaches the maximum growth and the water cycle is effectively closed [97–101]. The formation of cumulus clouds largely forced the dates and times of imaging chosen in the present study in the area of interest. The weather limitation is, in this case, a significant disadvantage for the proposed method of monitoring the soil hydraulic properties. On the other hand, the situation in different geographical areas may differ significantly.

The choice of a suitable imaging date is also important when it comes to the development of the vegetation cover of the area. As expected, the stand should be developed with sufficient leaf area, connected and developed with maximum water demand [102]. A stand with a developed root system should also identify spatial differences in the hydropedological properties of subsoil and water availability [85]. Likewise, Kroener et al. [103] reported that water uptake by roots was affected greatly by the hydraulic properties of the rhizosphere so that the reduced hydraulic conductivity mitigated the effects of drought stress. However, lower K_s was a good indicator of low-yielding zones [7]. The density of a vegetation is then important to limit the influence of the soil surface on the spectral information of the scanned space. The K_s and *FWC* values for the topsoil layer showed a good agreement of the measured and modeled values in the areas where the vegetation was dense for most of the evaluated sites (see Figure 6a) and Table 3). A surprising result was a very high correlation of the modeled and measured *FWC* values for the topsoil layer of the Makytí locality, which had minimal vegetation cover at the time of imaging (in both terms). The high correlation may be the effect of the spectral manifestation of the soil surface and the spatial heterogeneity of dry surface heating; however, this hypothesis needs to be verified.

The development of vegetation cover is essential for identifying hydropedological properties of the soil not only in the topsoil layer, but also in the subsoil. In this respect, in addition to soil properties (soil compaction, gleying, etc.), the development of the root system and the depth to which it extends are crucial. If the vegetation cover was limited (Makytí locality), a low correlation was found between the measured and modeled *FWC* values. The connection between the deeper soil layer and the surface that the plants are intended to show was not provided. Similarly, using deep-rooting plants, such as clover (U Mouček locality), can be problematic. Clover can obtain water from great depths (up to 2 m), so by its manifestation, they can effectively mask the lack of water in topsoil and shallow subsoil [104]. Due to the shallow subsoil of the U Mouček locality (35–55 cm), the more developed root system of the cereal–leguminous mixture will likely be more important, compared to monoculture [105].

The evaluation of areas with winter wheat showed, in most cases, a relatively high correlation for the measured and modeled *FWC* values in the subsoil layer. An exception is the Za Vaněčkovi locality, where the low correlation was probably due to a very complicated pedological situation. The results of *FWC* prediction for subsoil layer summarise Table 4

and Figure 6b). A large part of the land is systematically drained (61% of the area), and part of it are Eutric/Dystric Stagnic Cambisols and Eutric/Dystric Stagnosol (see Figure 2). Systematic drainage means, in addition to the actual change in the infiltration capacity of the soil, also a change in the composition of the soil profile, which, due to the mixing of soil layers during the deposition of drainage pipes, led to the formation of an anthroposoil (see [18] for more details).

4.2. Estimation of K_s and FWC Data from Aerial Imaging

The presented approach to estimating the K_s and *FWC* using RS data is based on the simple assumption that the development of crop water stress is defined by the rate of water infiltration into the soil. We can say that the higher the rate of infiltration, the faster the soil profile dries out and the faster the crop water stress occurs. Plant water stress is manifested by physiological changes, in the short term mainly by reducing transpiration and changing the energy balance of its surface [56,106]. The definition of the intensity of plant water stress is based on the change of temperature manifestation of the canopy, depending on the change in the energy exchange between the plants and the atmosphere, using the CWSI. The CWSI is a commonly used indicator, e.g., for irrigation purposes [107–110]. A significant advantage of the CWSI is the possibility of determination based on the spatial change of the temperature gradient within the observed space [57,111–115], so no further detailed supplementary data are needed. The calculation method is straightforward, and the agreement with the approach based on the theoretical basis, which was used in this work, is usually very good [111,112]. In this regard, this approach is easy to use in practice, without the need to know the physical nature of the derivation of the CWSI.

Although the hypothesis of a relationship between the CWSI and soil hydraulic properties is justified, data analysis has shown that the CWSI alone for the K_s and *FWC* estimation is insufficient. Other crop properties play an important role in the estimation of the hydraulic features. It is mainly the amount of crop biomass, its density, health status, or surface moisture. For this reason, the MSAVI and NDMI vegetation spectral indices were used in the prediction models. The MSAVI vegetation index makes it possible to describe the amount and state of biomass of the monitored stand [65,66]. The NDMI vegetation index significantly correlates with the vegetation surface moisture [67]. In both cases, the indices were used as covariates, making it easier to describe the complexity of the process by the model. The procedure of the *ad hoc* definition of the model variables was chosen. In contrast, when it comes to creating the smallest possible parsimony model, the approach of the so-called *forward selection* of variables was used, which was gradually added to the model. The minimum size of the model was chosen, given the amount of data used, among other things.

The amount of data used is one of the critical indicators when using machine learning methods. However, the SVR method used is one of the less sensitive methods applied to handle the used amount of data. As Al-Anazi and Gates [116] show, the sensitivity of the SVR models, particularly with the usage of the RBF kernel, is relatively low with respect to the size of the sample populations. In this work, the number of samples taken to determine the *FWC* for the individual sites was around 20; for the determination of the K_s, data from 31 measurement points were used. The number of values used in this study was considered sufficient for evaluating the spatial variability of soil hydraulic properties, given the realistic time, technical and economic possibilities of sampling for laboratory analyses at the monitored sites. An exception is the Kazy site, where only 11 samples were taken to determine the *FWC*, which can be considered a limit value. The resulting R^2 values may probably overestimate the real result in the case of a small volume of calibration data.

In comparison with published works, the presented results provide a comparable estimate of the observed characteristics of soil hydraulic properties, e.g., Ambrosone et al. [39] report $R^2 = 0.73$ for the linear method to determine soil water content, using multispectral data from the Sentinel 2 satellite and the OPTRAM model [117], and $R^2 = 0.8$ for the nonlinear method. Francos et al. [33] performed a detailed analysis of the spectral characteristics

of soils in relation to the infiltration rate. The results showed a very good agreement between laboratory and spectral data; however, the result varied according to the different types of soils and their physical properties. Haberle et al. [27] showed a very good agreement between the FWC and the RGB index derived from multispectral UAV images for the localities in the lower Jizera area (localities Kochánky and Sojovice). The values of the regression coefficient ranged between around 0.8 and 0.9, depending on the examined soil layer. It should be noted that the very high spatial resolution of the used images, which were able to capture sudden spatial changes of the spectral properties of the stand and soil properties, played a significant role in the evaluation. Methods based on thermal spatial data provided similar results as in previous cases, e.g., Boulet et al. [37], using the evaporation test, showed very good agreement with the data measured in situ. Similarly, Maltese et al. [36,118] described a very good agreement between soil bulk moisture values and values derived using the thermal inertia method.

The present method eliminates some of the limitations of the above approaches. In monitoring soil without vegetation cover using optical spectral data, the structural properties of soils and the content of color elements, such as hematite or goethite, can play an important role, which can significantly affect the spectral information [33]. Evaluation of soil hydraulic properties using spectral vegetation indices (e.g., the RGB index, [27]) may have only a limited possibility to identify short-term changes in the stand water regime. This approach is suitable for monitoring the manifestation of long-term changes. Methods based on evaluating the thermal properties of the stand and the soil surface, such as the evaporation test or the thermal inertia method, are approaches that are very sensitive to short-term changes in the soil hydraulic properties. The disadvantage is the need to obtain supplementary data (e.g., meteorological data) during imaging and usually a complicated calculation method. In addition, in determining the thermal inertia, it is necessary to perform imaging repeatedly during the day (for more details, see [35,36,118]).

The advantage of the presented method is the relative simplicity of calculating the commonly used spectral vegetation indices and the CWSI without requiring a large amount of supplementary data. Furthermore, since it is a method based on thermal data, the method is sensitive to short-term changes in the water regime of the stand. The nonlinear regression method allows a fairly good estimate of complex hydraulic soil properties, which are determined and influenced by several factors. The SVR method then provides the possibility to evaluate soil hydraulic properties, even based on a relatively small number of soil samples taken and analyzed, thereby increasing the efficiency of the spatial analysis of the studied areas. Due to its relative simplicity, the present method can be a suitable tool for evaluating the spatial variability of soil hydraulic properties and can, therefore, be applied in precision agriculture and protection of surface waters against the leaching of nutrients, especially nitrates.

5. Conclusions

Estimating soil hydraulic characteristics (the K_s and *FWC*) by the SVR, using a combination of the CWSI and vegetation indices obtained from aerial imaging, showed a good agreement with the measured data for most study sites. The analysis showed a good agreement between the measured and estimated Ks values for the observed areas (R^2 = 0.77). In the case of the evaluation of only the area of Za Vaněčkovi, the regression coefficient value was even R^2 = 0.96. Comparison of measured and estimated *FWC* values showed good results for the topsoil, while slightly worse results were found for the subsoil. In the first case, the values of the regression coefficient ranged from R^2 = 0.38 to R^2 = 0.99, and in the second case, from R^2 = 0.12 to R^2 = 0.99. The results showed the specific response of the individual study areas. Therefore, it is necessary to evaluate each study area separately to evaluate the hydraulic properties of soils.

Several factors influence the resulting relationship between the measured values of soil hydraulic properties and the values estimated from RS data. Of particular importance for the assessment is the state of development of the water stress of the vegetation. As

expected, stand water stress, expressed as the CWSI, is the main indicator of soil hydraulic properties. On the other hand, other stand properties, such as stand biomass (defined by the MSAVI spectral index) and possibly stand moisture (expressed by the NDMI index), need to be considered to assess the soil properties.

The quality of the RS data and the quality and quantity of the ground measurement data are important conditions for evaluating the soil hydraulic features. In the case of K_s, the number of measurements on individual fields is limited mainly by the measurements' complexity and time, technical and financial requirements. The imaging timing also appears to be crucial, with the optimal period being that of fully developed vegetation cover. The possibility of assessing areas without vegetation cover remains an open question. The time of imaging is also important for the use of RS data. Too early imaging may be influenced by dew, which may mask the expression of water stress in the crop cover. The soil environment also plays an important role, which can significantly affect the assessment outcome, e.g., the crop, previous and current agronomy, and drainage.

An issue for the assessment of soil properties is the spatial resolution of the sensors used. In the present work, data with a spatial resolution of 5×5 m were used. This resolution is probably sufficient for soil assessment in most cases. On the other hand, as shown by Haberle et al. [27,28], soil properties can change suddenly within units of meters. In this perspective, UAV technology with a very high resolution appears to be potentially applicable in practice. Alternatively, a combination of satellite (e.g., Sentinel 2) and UAV thermal data could be used in practical applications. The disadvantage of the proposed approach is the need for a combination of optical data in the visible and infrared spectral domain and thermal data. The problem is that most of the available systems do not provide complete data for estimating soil hydraulic properties, or only data with the insufficient spatial resolution are available, e.g., Landsat and MODIS. On the other hand, the application of commonly used spectral vegetation indices is an advantage of the proposed method.

The use of artificial intelligence methods (ML and DL) brings the possibility of analyzing (not only) soil hydraulic properties without the need for a priori knowledge of complex relationships between the biophysical manifestation of the surface (vegetation) and the soil hydraulic properties. This approach opens up new opportunities for the research and understanding of the relationships between soil, vegetation and atmosphere. Precision agriculture and its strategies are an important area of the application of AI methods in this respect.

Author Contributions: Conceptualization, J.B., R.D., A.Z., V.N. and J.H.; methodology, J.B., A.Z., R.D., V.N. and J.H.; software, J.B.; formal analysis, J.B.; investigation, J.B., R.D. and J.H.; resources, J.B., R.D., V.N., A.Z., J.H., K.K. and T.B.; data curation, J.B. and R.D.; writing—original draft preparation, J.B., R.D, J.H and V.N.; writing—review and editing, J.B., R.D., J.H., K.K., T.B.; visualization, V.N. and J.B.; project administration, R.D., J.B and J.H.; funding acquisition, R.D. All authors have read and agreed to the published version of the manuscript

Institutional Review Board Statement: Not applicable.

Informed Consent Statement: Not applicable.

Data Availability Statement: The data used for this work are not publicly available.

Conflicts of Interest: The authors declare no conflict of interest.

References

1. Castellini, M.; Di Prima, S.; Moret-Fernández, D.; Lassabatere, L. Rapid and accurate measurement methods for determining soil hydraulic properties: A review. *J. Hydrol. Hydromech.* **2021**, *69*, 121–139, doi:10.2478/johh-2021-0002.
2. Bayabil, H.K.; Dile, Y.T.; Tebebu, T.Y.; Engda, T.A.; Steenhuis, T.S. Evaluating infiltration models and pedotransfer functions: Implications for hydrologic modeling. *Geoderma* **2019**, *338*, 159–169, doi:10.1016/j.geoderma.2018.11.028.
3. Sihag, P.; Tiwari, N.; Ranjan, S. Estimation and inter-comparison of infiltration models. *Water Sci.* **2017**, *31*, 34–43, doi:10.1016/j.wsj.2017.03.001.
4. Kim, H.; Anderson, S.; Motavalli, P.; Gantzer, C. Compaction effects on soil macropore geometry and related parameters for an arable field. *Geoderma* **2010**, *160*, 244–251, doi:10.1016/j.geoderma.2010.09.030.
5. Shukla, M.K.; Slater, B.K.; Lal, R.; Cepuder, P. Spatial variability of soil properties and potential management classification of a chernozemic field in lower Austria. *Soil Sci.* **2004**, *169*, 852–860, doi:10.1097/00010694-200412000-00004.
6. Jabro, J.D.; Evans, R.G.; Kim, Y.; Iversen, W.M. Estimating in situ soil–water retention and field water capacity in two contrasting soil textures. *Irrig. Sci.* **2009**, *27*, 223–229, doi:10.1007/s00271-008-0137-9.
7. Keller, T.; Sutter, J.A.; Nissen, K.; Rydberg, T. Using field measurement of saturated soil hydraulic conductivity to detect low-yielding zones in three Swedish fields. *Soil Tillage Res.* **2012**, *124*, 68–77, doi:10.1016/j.still.2012.05.002.
8. Van Alphen, B.J.; Stoorvogel, J.J. A Functional approach to soil characterization in support of precision agriculture. *Soil Sci. Soc. Am. J.* **2000**, *64*, 1706–1713, doi:10.2136/sssaj2000.6451706x.
9. Usowicz, B.; Lipiec, J. Spatial variability of saturated hydraulic conductivity and its links with other soil properties at the regional scale. *Sci. Rep.* **2021**, *11*, 8293, doi:10.1038/s41598-021-86862-3.
10. Maleki, M.; Mouazen, A.; De Ketelaere, B.; Ramon, H.; De Baerdemaeker, J. On-the-go variable-rate phosphorus fertilisation based on a visible and near-infrared soil sensor. *Biosyst. Eng.* **2008**, *99*, 35–46, doi:10.1016/j.biosystemseng.2007.09.007.
11. Li, Y.; Shi, Z.; Li, F.; Li, H.Y. Delineation of site-specific management zones using fuzzy clustering analysis in a coastal saline land. *Comput. Electron. Agric.* **2007**, *56*, 174–186, doi:10.1016/j.compag.2007.01.013.
12. Koch, B.; Khosla, R.; Frasier, W.M.; Westfall, D.G.; Inman, D. Economic feasibility of variable-rate nitrogen application utilizing site-specific management zones. *Agron. J.* **2004**, *96*, 1572–1580, doi:10.2134/agronj2004.1572.
13. Casa, R.; Cavalieri, A.; Lo Cascio, B. Nitrogen fertilisation management in precision agriculture: a preliminary application example on maize. *Ital. J. Agron.* **2011**, *6*, 5, doi:10.4081/ija.2011.e5.
14. Kvítek, T.; Žlábek, P.; Bystřický, V.; Fučík, P.; Lexa, M.; Gergel, J.; Novák, P.; Ondr, P. Changes of nitrate concentrations in surface waters influenced by land use in the crystalline complex of the Czech Republic. *Phys. Chem. Earth Parts A/B/C* **2009**, *34*, 541–551, doi:10.1016/j.pce.2008.07.003.
15. Doležal, F.; Kvítek, T. The role of recharge zones, discharge zones, springs and tile drainage systems in peneplains of Central European highlands with regard to water quality generation processes. *Phys. Chem. Earth Parts A/B/C* **2004**, *29*, 775–785, doi:10.1016/j.pce.2004.05.005.
16. Duffková, R.; Fučík, P.; Jurkovská, L.; Janoušková, M. Experimental evaluation of the potential of arbuscular mycorrhiza to modify nutrient leaching in three arable soils located on one slope. *Appl. Soil Ecol.* **2019**, *143*, 116–125, doi:10.1016/j.apsoil.2019.06.001.
17. Fučík, P.; Zajíček, A.; Duffková, R.; Kvítek, T. *Water Quality of Agricultural Drainage Systems in the Czech Republic—Options for Its Improvement*; IntechOpen: London, UK, 2015; doi:10.5772/59298.
18. Duffková, R.; Zajíček, A.; Nováková, E. Actual evapotranspiration from partially tile-drained fields as influenced by soil properties, terrain and crop. *Soil Water Res.* **2011**, *6*, 131–146, doi:10.17221/20/2010-SWR.
19. Zajíček, A.; Kvítek, T.; Kaplická, M.; Doležal, F.; Kulhavý, Z.; Bystřický, V.; Žlábek, P. Drainage water temperature as a basis for verifying drainage runoff composition on slopes. *Hydrol. Process.* **2011**, *25*, 3204–3215, doi:10.1002/hyp.8039.
20. Fučík, P.; Zajíček, A.; Kaplická, M.; Duffková, R.; Peterková, J.; Maxová, J.; Takáčová, Š. Incorporating rainfall-runoff events into nitrate-nitrogen and phosphorus load assessments for small tile-drained catchments. *Water* **2017**, *9*, 712, doi:10.3390/w9090712.
21. Fabiani, S.; Vanino, S.; Napoli, R.; Zajíček, A.; Duffková, R.; Evangelou, E.; Nino, P. Assessment of the economic and environmental sustainability of Variable Rate Technology (VRT) application in different wheat intensive European agricultural areas. A Water energy food nexus approach. *Environ. Sci. Policy* **2020**, *114*, 366–376, doi:10.1016/j.envsci.2020.08.019.
22. Thorup-Kristensen, K.; Halberg, N.; Nicolaisen, M.; Olesen, J.E.; Crews, T.E.; Hinsinger, P.; Kirkegaard, J.; Pierret, A.; Dresbøll, D.B. Digging deeper for agricultural resources, the value of deep rooting. *Trends Plant Sci.* **2020**, *25*, 406–417, doi:10.1016/j.tplants.2019.12.007.
23. Saxton, K.E.; Rawls, W.J. Soil water characteristic estimates by texture and organic matter for hydrologic solutions. *Soil Sci. Soc. Am. J.* **2006**, *70*, 1569–1578. doi:10.2136/sssaj2005.0117.
24. Rasoulzadeh, A.; Fatemi, M. Scaling of cumulative infiltration curves using pedotransfer functions. In Proceedings of the 2011 International Conference on New Technology of Agricultural, IEEE, Zibo, China, 27–29 May 2011; pp. 646–650. doi:10.1109/ICAE.2011.5943879.
25. Abdelbaki, A.M.; Youssef, M.A.; Naguib, E.M.F.; Kiwan, M.E.; El-giddawy, E.I. Evaluation of pedotransfer functions for predicting saturated hydraulic conductivity for U.S. soils. In *2009 Reno, Nevada, 2009 Reno, Nevada, June 21—June 24, 2009*; American Society of Agricultural and Biological Engineers: St. Joseph Charter Township, MI, USA, 2009. doi:10.13031/2013.27309.
26. Novotný, M.; Kervališvili, D.; Šanta, M. *Irrigation of Field and Special Crops*, 1st ed.; Príroda: Bratislava, Slovakia, 2000.

27. Haberle, J.; Kurešová, G.; Křížová, K.; Lukáš, J.; Svoboda, P.; Raimanová, I.; Stehlík, M. Maps of spatial variability of soil water capacity. In *Hospodaření s Vodou v Krajině*; Rožnovský, J., Ed.; Česká Bioklimatologická Společnost: Třeboň, Czech Republic, 2020; p. 14. (In Czech)

28. Haberle, J.; Duffková, R.; Raimanová, I.; Fučík, P.; Svoboda, P.; Lukas, V.; Kurešová, G. The 13C discrimination of crops identifies soil spatial variability related to water shortage vulnerability. *Agronomy* **2020**, *10*, 1691, doi:10.3390/agronomy10111691.

29. Preza Fontes, G.; Bhattarai, R.; Christianson, L.E.; Pittelkow, C.M. Combining Environmental Monitoring and Remote Sensing Technologies to Evaluate Cropping System Nitrogen Dynamics at the Field-Scale. *Front. Sustain. Food Syst.* **2019**, *3*, 8, doi:10.3389/fsufs.2019.00008.

30. Sigler, W.A.; Ewing, S.A.; Jones, C.A.; Payn, R.A.; Miller, P.; Maneta, M. Water and nitrate loss from dryland agricultural soils is controlled by management, soils, and weather. *Agric. Ecosyst. Environ.* **2020**, *304*, 107158, doi:10.1016/j.agee.2020.107158.

31. Yang, Y.; Zhang, J.; Bao, Z.; Ao, T.; Wang, G.; Wu, H.; Wang, J. Evaluation of multi-source soil moisture datasets over central and eastern agricultural area of China using in situ monitoring network. *Remote. Sens.* **2021**, *13*, 1175, doi:10.3390/rs13061175.

32. Kornelsen, K.C.; Coulibaly, P. Advances in soil moisture retrieval from synthetic aperture radar and hydrological applications. *J. Hydrol.* **2013**, *476*, 460–489, doi:10.1016/j.jhydrol.2012.10.044.

33. Francos, N.; Romano, N.; Nasta, P.; Zeng, Y.; Szabó, B.; Manfreda, S.; Ciraolo, G.; Mészáros, J.; Zhuang, R.; Su, B.; Ben-Dor, E. Mapping water infiltration rate using ground and UAV hyperspectral data: A case study of Alento, Italy. *Remote Sens.* **2021**, *13*, 2606, doi:10.3390/rs13132606.

34. Wu, D.H.; Fan, W.J.; Cui, Y.K.; Yan, B.Y.; Xu, X.R. Review of monitoring soil water content using hyperspectral remote sensing. *Spectrosc. Spectr. Anal.* **2010**, *30*, 3067–3071.

35. Sobrino, J.; El Kharraz, M. Combining afternoon and morning NOAA satellites for thermal inertia estimation: 2. Methodology and application. *J. Geophys. Res. Atmos.* **1999**, *104*, 9455–9465.

36. Maltese, A.; Bates, P.; Capodici, F.; Cannarozzo, M.; Ciraolo, G.; La Loggia, G. Critical analysis of thermal inertia approaches for surface soil water content retrieval. *Hydrol. Sci. J.* **2013**, *58*, 1144–1161, doi:10.1080/02626667.2013.802322.

37. Boulet, G.; Mougenot, B.; Abdelouahab, T.B. An evaporation test based on Thermal Infra Red remote-sensing to select appropriate soil hydraulic properties. *J. Hydrol.* **2009**, *376*, 589–598, doi:10.1016/j.jhydrol.2009.07.068.

38. Sadeghi, M.; Babaeian, E.; Tuller, M.; Jones, S.B. The optical trapezoid model: A novel approach to remote sensing of soil moisture applied to Sentinel-2 and Landsat-8 observations. *Remote. Sens. Environ.* **2017**, *198*, 52–68, doi:10.1016/j.rse.2017.05.041.

39. Ambrosone, M.; Matese, A.; Di Gennaro, S.F.; Gioli, B.; Tudoroiu, M.; Genesio, L.; Miglietta, F.; Baronti, S.; Maienza, A.; Ungaro, F.; Toscano, P. Retrieving soil moisture in rainfed and irrigated fields using Sentinel-2 observations and a modified OPTRAM approach. *Int. J. Appl. Earth Obs. Geoinf.* **2020**, *89*, 102113, doi:10.1016/j.jag.2020.102113.

40. Neale, C.M.; Geli, H.M.; Kustas, W.P.; Alfieri, J.G.; Gowda, P.H.; Evett, S.R.; Prueger, J.H.; Hipps, L.E.; Dulaney, W.P.; Chávez, J.L.; et al. Soil water content estimation using a remote sensing based hybrid evapotranspiration modeling approach. *Adv. Water Resour.* **2012**, *50*, 152–161.

41. Nemani, R.; Pierce, L.; Running, S.; Goward, S. Developing satellite-derived estimates of surface moisture status. *J. Appl. Meteorol. Climatol.* **1993**, *32*, 548–557, doi:10.1175/1520-0450(1993)032<0548:DSDEOS>2.0.CO;2.

42. Zhang, D.; Tang, R.; Zhao, W.; Tang, B.; Wu, H.; Shao, K.; Li, Z.L. Surface soil water content estimation from thermal remote sensing based on the temporal variation of land surface temperature. *Remote Sens.* **2014**, *6*, 3170–3187.

43. Lary, D.J.; Alavi, A.H.; Gandomi, A.H.; Walker, A.L. Machine learning in geosciences and remote sensing. *Geosci. Front.* **2016**, *7*, 3–10, doi:10.1016/j.gsf.2015.07.003.

44. Xu, C.; Jackson, S.A. Machine learning and complex biological data. *Genome Biol.* **2019**, *20*, 76, doi:10.1186/s13059-019-1689-0.

45. Ahmad, S.; Kalra, A.; Stephen, H. Estimating soil moisture using remote sensing data: A machine learning approach. *Adv. Water Resour.* **2010**, *33*, 69–80, doi:10.1016/j.advwatres.2009.10.008.

46. Ali, I.; Greifeneder, F.; Stamenkovic, J.; Neumann, M.; Notarnicola, C. Review of Machine Learning approaches for biomass and soil moisture retrievals from remote sensing data. *Remote Sens.* **2015**, *7*, 16398–16421, doi:10.3390/rs71215841.

47. Cameira, M.; Mota, M. Nitrogen related diffuse pollution from horticulture production—mitigation practices and assessment strategies. *Horticulturae* **2017**, *3*, 25, doi:10.3390/horticulturae3010025.

48. Kvítek, T. (Ed.) *Retence a Jakost Vody v Povodí vodárenské nádrže Švihov na Želivce: Význam Retence Vody na zeměDělském půdním Fondu Pro Jakost Vody a Současně i průvodce Vodním režimem Krystalinika*, 2nd ed.; Povodí Vltavy, State Enterprise, Czech Republic: Prague, Czech Republic, 2018. (In Czech)

49. Tolasz, R. (Ed.) *Climate Atlas of Czechia*, 1st ed.; Czech Hydrometeorological Institute, Palacký University Olomouc: Prague, Olomouc, Czech Republic, 2007. (In Czech)

50. Žigová, A. Development of soils on paragneiss and granite in the southeastern part of Bohemia. *Acta Geodyn. Geomater.* **2013**, *10*, 85–95, doi:10.13168/AGG.2013.0008.

51. Serrano, S.E. *Hydrology for Engineers, Geologists, and Environmental Professionals: An Integrated Treatment of Surface, Subsurface, and Contaminant Hydrology*; HydroScience: Lexington, Fayette, 1997.

52. FAO. *World Reference Base for Soil Resources 2014, Update 2015: International Soil Classification System for Naming Soils and Creating Legends for Soil Maps. World Soil Resources Reports No. 106.*; FAO: Rome, Italy, 2015.

53. Bruthans, J.; Kůrková, I.; Kadlecová, R. Factors controlling nitrate concentration in space and time in wells distributed along an aquifer/river interface (Káraný, Czechia). *Hydrogeol. J.* **2019**, *27*, 195–210, doi:10.1007/s10040-018-1854-7.

54. Philip, J. Approximate analysis of the borehole permeameter in unsaturated soil. *Water Resour. Res.* **1985**, *21*, 1025–1033.
55. ISO 11277. *Soil Quality–Determination of Particle Size Distribution in Mineral Soil Material–Method by Sieving and Sedimentation*; International Organization for Standardization, Geneve, Switzerland, 2009.
56. Jackson, R.D.; Idso, S.B.; Reginato, R.J.; Pinter, P.J. Canopy temperature as a crop water stress indicator. *Water Resour. Res.* **1981**, *17*, 1133, doi:10.1029/WR017i004p01133.
57. Jackson, R.D.; Kustas, W.P.; Choudhury, B.J. A reexamination of the crop water stress index. *Irrig. Sci.* **1988**, *9*, 309–317.
58. Monin, A.; Obukhov, A. Basic laws of turbulent mixing in the atmosphere near the ground. *Tr. Akad. Nauk SSSR Geoph. Inst.* **1954**, *64*, 1963–1987.
59. Koloskov, G.; Mukhamejanov, K.; Tanton, T. Monin–Obukhov length as a cornerstone of the SEBAL calculations of evapotranspiration. *J. Hydrol.* **2007**, *335*, 170–179, doi:10.1016/j.jhydrol.2006.11.010.
60. Monteith, J.L.; Unsworth, M.H. *Principles of Environmental Physics*, 2nd ed.; Butterworth-Heinemann: Oxford, UK, 1990.
61. Thom, A.S. Momentum, mass and heat exchange of plant communities. In *Vegetation and the Atmosphere, Principles*; Monteith, J.L., Ed.; Academic Press: London, UK, 1975; Volume. 1, pp. 57–110.
62. Beljaars, A.C.M.; Holtslag, A.a.M. Flux parameterization over land surfaces for atmospheric models. *J. Appl. Meteorol. Climatol.* **1991**, *30*, 327–341, doi:10.1175/1520-0450(1991)030<0327:FPOLSF>2.0.CO;2.
63. Brutsaert, W. *Evaporation into the Atmosphere: Theory, History, and Applications*; Environmental Fluid Mechanics, Reidel Publishing Company: Dordrecht, The Netherland; Boston, MA, USA, 1982.
64. Jarvis, P.; McNaughton, K. Stomatal control of transpiration: Scaling up from leaf to region. In *Advances in Ecological Research*; Elsevier: Hoboken, NJ, USA, 1986; Volume15, pp. 1–49.
65. Qi, J.; Chehbouni, A.; Huete, A.; Kerr, Y.; Sorooshian, S. A modified soil adjusted vegetation index. *Remote. Sens. Environ.* **1994**, *48*, 119–126, doi:10.1016/0034-4257(94)90134-1.
66. Gao, Z.Q.; Liu, C.S.; Gao, W.; Chang, N.B. A coupled remote sensing and the Surface Energy Balance with Topography Algorithm (SEBTA) to estimate actual evapotranspiration over heterogeneous terrain. *Hydrol. Earth Syst. Sci.* **2011**, *15*, 119–139, doi:10.5194/hess-15-119-2011.
67. Jin, S.; Sader, S. Comparison of time series tasseled cap wetness and the normalized difference moisture index in detecting forest disturbances. *Remote. Sens. Environ.* **2005**, *94*, 364–372, doi:10.1016/j.rse.2004.10.012.
68. Hatfield, J.L.; Gitelson, A.A.; Schepers, J.S.; Walthall, C.L. Application of Spectral remote sensing for agronomic decisions. *Agron. J.* **2008**, *100*, S-117–S-131, doi:10.2134/agronj2006.0370c.
69. Peñuelas, J.; Filella, I. Visible and near-infrared reflectance techniques for diagnosing plant physiological status. *Trends Plant Sci.* **1998**, *3*, 151–156, doi:10.1016/S1360-1385(98)01213-8.
70. Jaafar, H.H.; Ahmad, F.A. Time series trends of Landsat-based ET using automated calibration in METRIC and SEBAL: The Bekaa Valley, Lebanon. *Remote. Sens. Environ.* **2020**, *238*, 111034, doi:10.1016/j.rse.2018.12.033.
71. Huete, A. A soil-adjusted vegetation index (SAVI). *Remote. Sens. Environ.* **1988**, *25*, 295–309, doi:10.1016/0034-4257(88)90106-X.
72. Brom, J. SEBCS for QGIS-Module for Calculation of Energy Balance Features and Vegetation Water Stress Indices. 2021. Available online: https://github.com/JakubBrom/SEBCS (accessed on 20 May 2021).
73. Cortes, C.; Vapnik, V. Support-vector networks. *Mach. Learn.* **1995**, *20*, 273–297, doi:10.1007/BF00994018.
74. Drucker, H.; Burges, C.J.; Kaufman, L.; Smola, A.; Vapnik, V. Support vector regression machines. *Adv. Neural Inf. Process. Syst.* **1997**, *9*, 155–161.
75. Meyer, D.; Dimitriadou, E.; Hornik, K.; Weingessel, A.; Leisch, F. *e1071: Misc Functions of the Department of Statistics, R Package Version 1.7-7*; Probability Theory Group (Formerly: E1071), TU Wien; Probability Theory Group: Leiden, The Netherlands, 2021.
76. R Core Team. *R: A Language and Environment for Statistical Computing*; R Foundation for Statistical Computing: Vienna, Austria, 2021.
77. Arrington, K.E.; Ventura, S.J.; Norman, J.M. Predicting saturated hydraulic conductivity for estimating maximum soil infiltration rates. *Soil Sci. Soc. Am. J.* **2013**, *77*, 748–758, doi:10.2136/sssaj2012.0288.
78. Jadczyszyn, J.; Niedźwiecki, J. Relation of saturated hydraulic conductivity to soil losses. *Pol. J. Environ. Stud.* **2005**, *14*, 431–435.
79. Ahiablame, L.; Chaubey, I.; Smith, D.; Engel, B. Effect of tile effluent on nutrient concentration and retention efficiency in agricultural drainage ditches. *Agric. Water Manag.* **2011**, *98*, 1271–1279, doi:10.1016/j.agwat.2011.03.002.
80. Kühling, I.; Beiküfner, M.; Vergara, M.; Trautz, D. Effects of adapted N-fertilisation strategies on nitrate leaching and yield performance of arable crops in North-Western Germany. *Agronomy* **2020**, *11*, 64, doi:10.3390/agronomy11010064.
81. Edwards, W.M.; Shipitalo, M.J.; Owens, L.B.; Dick, W.A. Factors affecting preferential flow of water and atrazine through earthworm burrows under continuous no-till corn. *J. Environ. Qual.* **1993**, *22*, 453–457, doi:10/df2d4n.
82. Jabro, J.; Stevens, W.B.; Evans, R.G.; Iversen, W.M. Spatial variability and correlation of selected soil properties in the Ap horizon of a CRP grassland. *Appl. Eng. Agric.* **2010**, *26*, 419–428, doi:10.13031/2013.29957.
83. Smith, E.A.; Capel, P.D. Specific conductance as a tracer of preferential flow in a subsurface-drained field. *Vadose Zone J.* **2018**, *17*, 170206, doi:10.2136/vzj2017.11.0206.
84. Jabro, J.D.; Stevens, B.W.; Evans, R.G. Spatial relationships among soil physical properties in a grass-alfalfa hay field. *Soil Sci.* **2006**, *171*, 719–727, doi:10.1097/01.ss.0000228044.87894.aa.

85. Zhang, X.X.; Whalley, P.A.; Ashton, R.W.; Evans, J.; Hawkesford, M.J.; Griffiths, S.; Huang, Z.D.; Zhou, H.; Mooney, S.J.; Whalley, W.R. A comparison between water uptake and root length density in winter wheat: effects of root density and rhizosphere properties. *Plant Soil* **2020**, *451*, 345–356, doi:10.1007/s11104-020-04530-3.

86. Dušek, J.; Vogel, T. Modeling subsurface hillslope runoff dominated by preferential flow: One- vs. two-dimensional approximation. *Vadose Zone J.* **2014**, *13*, vzj2013.05.0082, doi:10.2136/vzj2013.05.0082.

87. Hlaváčiková, H.; Novák, V.; Holko, L. On the role of rock fragments and initial soil water content in the potential subsurface runoff formation. *J. Hydrol. Hydromech.* **2015**, *63*, 71–81, doi:10.1515/johh-2015-0002.

88. Lin, J.; Govindaraju, R. *Conductivity of Soils with Preferential Flow Paths*; Technical Report; Kansas State Univ.: Manhattan, KS, USA, 1996.

89. Němeček, J.; Muhlhanselová, M.; Macků, J.; Vokoun, J.; Vavříček, D.; Novák, P. *The Czech Taxonomic Soil Classification System*, 2nd ed.; Czech University of Life Science Prague: Prague, Czech Republic, 2011.

90. Zajíček, A.; Pomije, T.; Kvítek, T. Event water detection in tile drainage runoff using stable isotopes and a water temperature in small agricultural catchment in Bohemian-Moravian Highlands, Czech Republic. *Environ. Earth Sci.* **2016**, *75*, 838, doi:10.1007/s12665-016-5561-1.

91. Kadlecová, R.; Bruthans, J.; Grundloch, J.; Gvoždík, L.; Haberle, J.; Klír, J.; Kůrková, I.; Milický, M.; Růžek, P.; Herčík, L. *Kvartérní Sedimenty, Podzemní Voda a Zemědělství*; Výzkumný ústav rostlinné výroby, Česká geologická služba, ProGeo, and Pražské vodovody a kanalizace: Prague, Prague, 2018. (In Czech)

92. Munné-Bosch, S.; Alegre, L. Role of dew on the recovery of water-stressed *Melissa officinalis* L. plants. *J. Plant Physiol.* **1999**, *154*, 759–766, doi:10.1016/S0176-1617(99)80255-7.

93. Gerlein-Safdi, C.; Koohafkan, M.C.; Chung, M.; Rockwell, F.E.; Thompson, S.; Caylor, K.K. Dew deposition suppresses transpiration and carbon uptake in leaves. *Agric. For. Meteorol.* **2018**, *259*, 305–316, doi:10.1016/j.agrformet.2018.05.015.

94. Vuollekoski, H.; Vogt, M.; Sinclair, V.A.; Duplissy, J.; Järvinen, H.; Kyrö, E.M.; Makkonen, R.; Petäjä, T.; Prisle, N.L.; Räisänen, P.; et al. Estimates of global dew collection potential on artificial surfaces. *Hydrol. Earth Syst. Sci.* **2015**, *19*, 601–613, doi:10.5194/hess-19-601-2015.

95. Del'Arco Sanches, I.; Feitosa, R.Q.; Achanccaray Diaz, P.M.; Dias Soares, M.; Barreto Luiz, A.J.; Schultz, B.; Pinheiro Maurano, L.E. Campo Verde database: Seeking to improve agricultural remote sensing of tropical areas. *IEEE Geosci. Remote. Sens. Lett.* **2018**, *15*, 369–373, doi:10.1109/LGRS.2017.2789120.

96. Green, E.P.; Mumby, P.J.; Edwards, A.J.; Clark, C.D. A review of remote sensing for the assessment and management of tropical coastal resources. *Coast. Manag.* **1996**, *24*, 1–40, doi:10.1080/08920759609362279.

97. Makarieva, A.M.; Gorshkov, V.G. Biotic pump of atmospheric moisture as driver of the hydrological cycle on land. *Hydrol. Earth Syst. Sci.* **2007**, *11*, 1013–1033, doi:10.5194/hess-11-1013-2007.

98. Makarieva, A.M.; Gorshkov, V.G.; Li, B.L. Conservation of water cycle on land via restoration of natural closed-canopy forests: implications for regional landscape planning. *Ecol. Res.* **2006**, *21*, 897–906, doi:10.1007/s11284-006-0036-6.

99. Makarieva, A.M.; Gorshkov, V.G. The Biotic Pump: condensation, atmospheric dynamics and climate. *Int. J. Water* **2010**, *5*, 365, doi:10.1504/IJW.2010.038729.

100. Hesslerová, P.; Pokorný, J.; Brom, J.; Rejšková-Procházková, A. Daily dynamics of radiation surface temperature of different land cover types in a temperate cultural landscape: consequences for the local climate. *Ecol. Eng.* **2013**, *54*, 145–154, doi:10.1016/j.ecoleng.2013.01.036.

101. Huryna, H.; Pokorný, J. The role of water and vegetation in the distribution of solar energy and local climate: a review. *Folia Geobot.* **2016**, *51*, 191–208, doi:10.1007/s12224-016-9261-0.

102. Allen, R.G.; Food and Agriculture Organization of the United Nations., Eds. *Crop Evapotranspiration: Guidelines for Computing Crop Water Requirements*; Number 56 in FAO Irrigation and Drainage Paper, Food and Agriculture Organization of the United Nations: Rome, Italy, 1998.

103. Kroener, E.; Zarebanadkouki, M.; Bittelli, M.; Carminati, A. Simulation of root water uptake under consideration of nonequilibrium dynamics in the rhizosphere: Water content dynamics in the rhizosphere. *Water Resour. Res.* **2016**, *52*, 5755–5770, doi:10.1002/2015WR018579.

104. Brown, H.; Moot, D.; Pollock, K. Long term growth rates and water extraction patterns of dryland chicory, lucerne and red clover. *NZGA: Res. Pract. Ser.* **2003**, *11*, 91–99, doi:10.33584/rps.11.2003.2991.

105. Haughey, E.; McElwain, J.C.; Finn, J.A. Variability of water supply affected shoot biomass and root depth distribution of four temperate grassland species in monocultures and mixtures. *J. Plant Ecol.* **2020**, *13*, 554–562, doi:10.1093/jpe/rtaa044.

106. Idso, S.B.; Jackson, R.D.; Reginato, R.J. Remote-sensing of crop yields. *Science* **1977**, *196*, 19–25, doi:10.1126/science.196.4285.19.

107. Alderfasi, A.A.; Nielsen, D.C. Use of crop water stress index for monitoring water status and scheduling irrigation in wheat. *Agric. Water Manag.* **2001**, *47*, 69–75, doi:10.1016/S0378-3774(00)00096-2.

108. Irmak, S.; Haman, D.Z.; Bastug, R. Determination of crop water stress index for irrigation timing and yield estimation of corn. *Agron. J.* **2000**, *92*, 1221–1227.

109. Sepaskhah, A.; Kashefipour, S. Relationships between leaf water potential, CWSI, yield and fruit quality of sweet lime under drip irrigation. *Agric. Water Manag.* **1994**, *25*, 13–21.

110. Nielsen, D. Scheduling irrigations for soybeans with the crop water stress index (CWSI). *Field Crop. Res.* **1990**, *23*, 103–116.

111. Gardner, B.R.; Nielsen, D.C.; Shock, C.C. Infrared thermometry and the crop water stress index. I. History, theory, and baselines. *J. Prod. Agric.* **1992**, *5*, 462–466, doi:10.2134/jpa1992.0462.

112. Gardner, B.R.; Nielsen, D.C.; Shock, C.C. Infrared thermometry and the crop water stress index. II. Sampling procedures and interpretation. *J. Prod. Agric.* **1992**, *5*, 466–475, doi:10.2134/jpa1992.0466.

113. Jones, H.G.; Stoll, M.; Santos, T.; de Sousa, M.; Chaves, M.M.; Grant, O.M. Use of infrared thermography for monitoring stomatal closure in the field: application to grapevine. *J. Exp. Bot.* **2002**, *53*, 2249–2260, doi:10.1093/jxb/erf083.

114. Jones, H.G.; Serraj, R.; Loveys, B.R.; Xiong, L.; Wheaton, A.; Price, A.H. Thermal infrared imaging of crop canopies for the remote diagnosis and quantification of plant responses to water stress in the field. *Funct. Plant Biol.* **2009**, *36*, 978, doi:10.1071/FP09123.

115. Leinonen, I.; Grant, O.M.; Tagliavia, C.P.P.; Chaves, M.M.; Jones, H.G. Estimating stomatal conductance with thermal imagery. *Plant Cell Environ.* **2006**, *29*, 1508–1518, doi:10.1111/j.1365-3040.2006.01528.x.

116. Al-Anazi, A.; Gates, I. Support vector regression to predict porosity and permeability: Effect of sample size. *Comput. Geosci.* **2012**, *39*, 64–76, doi:10.1016/j.cageo.2011.06.011.

117. Babaeian, E.; Sadeghi, M.; Franz, T.E.; Jones, S.; Tuller, M. Mapping soil moisture with the OPtical TRApezoid Model (OPTRAM) based on long-term MODIS observations. *Remote. Sens. Environ.* **2018**, *211*, 425–440, doi:10.1016/j.rse.2018.04.029.

118. Maltese, A.; Minacapilli, M.; Cammalleri, C.; Ciraolo, G.; D'Asaro, F. A thermal inertia model for soil water content retrieval using thermal and multispectral images. *Remote Sens.* **2010**, *7824*, 78241G.